Fermi National Accelerator Laboratory

FERMILAB-Pub-93/003-E

A Study of Four-Jet Events and Evidence for Double Parton Interactions in $p\bar{p}$ Collisions at $\sqrt{s} = 1.8$ TeV

F. Abe et al
The CDF Collaboration

Fermi National Accelerator Laboratory
P.O. Box 500, Batavia, Illinois 60510

January 1993

Submitted to *Physical Review D*

Operated by Universities Research Association Inc. under Contract No. DE-AC02-76CHO3000 with the United States Department of Energy

Disclaimer

CDF/PUB/JET/CDFR/1885
FERMILAB-PUB-93/003-E

A Study of Four-Jet Events and Evidence for Double Parton Interactions in $p\bar{p}$ collisions at $\sqrt{s} = 1.8$ TeV

F. Abe,[11] M. Albrow,[6] D. Amidei,[14] C. Anway-Wiese,[3] G. Apollinari,[22] M. Atac,[6] P. Auchincloss,[21] P. Azzi,[16] A. R. Baden,[8] N. Bacchetta,[15] W. Badgett,[14] M. W. Bailey,[20] A. Bamberger,[6,a] P. de Barbaro,[21] A. Barbaro-Galtieri,[12] V. E. Barnes,[20] B. A. Barnett,[10] G. Bauer,[13] T. Baumann,[8] F. Bedeschi,[19] S. Behrends,[2] S. Belforte,[19] G. Bellettini,[19] J. Bellinger,[27] D. Benjamin,[26] J. Benlloch,[6,a] J. Bensinger,[2] A. Beretvas,[6] J. P. Berge,[6] S. Bertolucci,[7] K. Biery,[17,a] S. Bhadra,[9] M. Binkley,[6] D. Bisello,[16] R. Blair,[1] C. Blocker,[2] A. Bodek,[21] V. Bolognesi,[19] A. W. Booth,[6] C. Boswell,[10] G. Brandenburg,[8] D. Brown,[8] E. Buckley-Geer,[6] H. S. Budd,[21] G. Busetto,[16] A. Byon-Wagner,[6] K. L. Byrum,[1] C. Campagnari,[6] M. Campbell,[14] A. Caner,[6] R. Carey,[8] W. Carithers,[12] D. Carlsmith,[27] J. T. Carroll,[6] R. Cashmore,[6,a] A. Castro,[16] F. Cervelli,[19] K. Chadwick,[6] J. Chapman,[14] G. Chiarelli,[7] W. Chinowsky,[12] S. Cihangir,[6] A. G. Clark,[6] M. Cobal,[19] D. Connor,[17] M. Contreras,[4] J. Cooper,[6] M. Cordelli,[7] D. Crane,[6] J. D. Cunningham,[2] C. Day,[6] F. DeJongh,[6] S. Dell'Agnello,[19] M. Dell'Orso,[19] L. Demortier,[22] B. Denby,[6] P. F. Derwent,[14] T. Devlin,[23] D. DiBitonto,[24] M. Dickson,[21] R. B. Drucker,[12] K. Einsweiler,[12] J. E. Elias,[6] R. Ely,[12] S. Eno,[4] S. Errede,[9] A. Etchegoyen,[6,a] B. Farhat,[13] M. Frautschi,[15] G. J. Feldman,[8] B. Flaugher,[6] G. W. Foster,[6] M. Franklin,[8] J. Freeman,[6] H. Frisch,[4] T. Fuess,[6] Y. Fukui,[11] A. F. Garfinkel,[20] A. Gauthier,[9] S. Geer,[6] D. W. Gerdes,[4] P. Giannetti,[19] N. Giokaris,[22] P. Giromini,[7] L. Gladney,[17] M. Gold,[15] J. Gonzalez,[17] K. Goulianos,[22] H. Grassmann,[16] G. M. Grieco,[19] R. Grindley,[17,a] C. Grosso-Pilcher,[4] C. Haber,[12] S. R. Hahn,[6] R. Handler,[27] K. Hara,[25] B. Harral,[17] R. M. Harris,[6] S. A. Hauger,[5] J. Hauser,[3] C. Hawk,[23] T. Hessing,[24] R. Hollebeek,[17] L. Holloway,[9] S. Hong,[14] G. Houk,[17] P. Hu,[18] B. Hubbard,[12] B. T. Huffman,[18] R. Hughes,[21] P. Hurst,[8] J. Huth,[6] J. Hylen,[6] M. Incagli,[19] T. Ino,[25] H. Iso,[25] H. Jensen,[6] C. P. Jessop,[8] R. P. Johnson,[6] U. Joshi,[6] R. W. Kadel,[12] T. Kamon,[25] S. Kanda,[25] D. A. Kardelis,[9] I. Karliner,[9] E. Kearns,[8] L. Keeble,[24] R. Kephart,[6] P. Kesten,[2] R. M. Keup,[9] H. Keutelian,[6] D. Kim,[6] S. B. Kim,[14] S. H. Kim,[25] Y. K. Kim,[12] L. Kirsch,[2] K. Kondo,[25] J. Konigsberg,[8] K. Kordas,[17,a] E. Kovacs,[6] M. Krasberg,[14] S. E. Kuhlmann,[1] E. Kuns,[23] A. T. Laasanen,[20] S. Lammel,[3] J. I. Lamoureux,[27] S. Leone,[19] J. D. Lewis,[6] W. Li,[1] P. Limon,[6] M. Lindgren,[3] T. M. Liss,[9] N. Lockyer,[17] M. Loreti,[16] E. H. Low,[17] D. Lucchesi,[19] C. B. Luchini,[9] P. Lukens,[6] P. Maas,[27] K. Maeshima,[6] M. Mangano,[19] J. P. Marriner,[6] M. Mariotti,[19] R. Markeloff,[27] L. A. Markosky,[27] J. Matthews,[15] R. Mattingly,[2] P. McIntyre,[24] A. Menzione,[19] E. Meschi,[19] T. Meyer,[24] S. Mikamo,[11] M. Miller,[4] T. Mimashi,[25] S. Miscetti,[7] M. Mishina,[11] S. Miyashita,[25] Y. Morita,[25] S. Moulding,[2] J. Mueller,[23] A. Mukherjee,[6] T. Muller,[3] L. F. Nakae,[2] I. Nakano,[25] C. Nelson,[6] D. Neuberger,[3] C. Newman-Holmes,[6] J. S. T. Ng,[8] M. Ninomiya,[25] L. Nodulman,[1] S. Ogawa,[25] R. Paoletti,[19] V. Papadimitriou,[6] A. Para,[6] E. Pare,[8] S. Park,[6] J. Patrick,[6] G. Pauletta,[19] L. Pescara,[16] G. Piacentino,[19] T. J. Phillips,[5] F. Ptohos,[8] R. Plunkett,[6] L. Pondrom,[27] J. Proudfoot,[1] G. Punzi,[19] D. Quarrie,[6] K. Ragan,[17,a] G. Redlinger,[4] J. Rhoades,[27] M. Roach,[26] F. Rimondi,[6,a] L. Ristori,[19] W. J. Robertson,[5] T. Rodrigo,[6] T. Rohaly,[17] A. Roodman,[4] W. K. Sakumoto,[21] A. Sansoni,[7] R. D. Sard,[9] A. Savoy-Navarro,[6] V. Scarpine,[9] P. Schlabach,[8] E. E. Schmidt,[6]

Submitted to Physical Review D, January 8, 1993.

O. Schneider,[12] M. H. Schub,[20] R. Schwitters,[8] A. Scribano,[19] S. Segler,[6] S. Seidel,[15] Y. Seiya,[25] G. Sganos,[17,a] M. Shapiro,[12] N. M. Shaw,[20] M. Sheaff,[27] M. Shochet,[4] J. Siegrist,[12] A. Sill,[21] P. Sinervo,[17,a] J. Skarha,[10] K. Sliwa,[26] D. A. Smith,[19] F. D. Snider,[10] L. Song,[6] T. Song,[14] M. Spahn,[12] A. Spies,[10] P. Sphicas,[13] R. St. Denis,[8] L. Stanco,[6,a] A. Stefanini,[19] G. Sullivan,[4] K. Sumorok,[13] R. L. Swartz, Jr.,[9] M. Takano,[25] K. Takikawa,[25] S. Tarem,[2] F. Tartarelli,[19] S. Tether,[13] D. Theriot,[6] M. Timko,[26] P. Tipton,[21] S. Tkaczyk,[6] A. Tollestrup,[6] J. Tonnison,[20] W. Trischuk,[8] Y. Tsay,[4] J. Tseng,[10] N. Turini,[19] F. Ukegawa,[25] D. Underwood,[1] S. Vejcik, III,[14] R. Vidal,[6] R. G. Wagner,[1] R. L. Wagner,[6] N. Wainer,[6] R. C. Walker,[21] J. Walsh,[17] G. Watts,[21] T. Watts,[23] R. Webb,[24] C. Wendt,[27] H. Wenzel,[19] W. C. Wester, III,[12] T. Westhusing,[9] S. N. White,[22] A. B. Wicklund,[1] E. Wicklund,[6] H. H. Williams,[17] B. L. Winer,[21] J. Wolinski,[24] D. Y. Wu,[14] X. Wu,[19] J. Wyss,[16] A. Yagil,[6] K. Yasuoka,[25] Y. Ye,[17,a] G. P. Yeh,[6] C. Yi,[17] J. Yoh,[6] M. Yokoyama,[25] J. C. Yun,[6] A. Zanetti,[19] F. Zetti,[19] S. Zhang,[14] W. Zhang,[16] S. Zucchelli,[6,a]

The CDF Collaboration

[1] *Argonne National Laboratory, Argonne, Illinois 60439*
[2] *Brandeis University, Waltham, Massachusetts 02254*
[3] *University of California at Los Angeles, Los Angeles, California 90024*
[4] *University of Chicago, Chicago, Illinois 60637*
[5] *Duke University, Durham, North Carolina 27706*
[6] *Fermi National Accelerator Laboratory, Batavia, Illinois 60510*
[7] *Laboratori Nazionali di Frascati, Istituto Nazionale di Fisica Nucleare, Frascati, Italy*
[8] *Harvard University, Cambridge, Massachusetts 02138*
[9] *University of Illinois, Urbana, Illinois 61801*
[10] *The Johns Hopkins University, Baltimore, Maryland 21218*
[11] *National Laboratory for High Energy Physics (KEK), Japan*
[12] *Lawrence Berkeley Laboratory, Berkeley, California 94720*
[13] *Massachusetts Institute of Technology, Cambridge, Massachusetts 02139*
[14] *University of Michigan, Ann Arbor, Michigan 48109*
[15] *University of New Mexico, Albuquerque, NM 87131*
[16] *Universita di Padova, Instituto Nazionale di Fisica Nucleare, Sezione di Padova, I-35131 Padova, Italy*
[17] *University of Pennsylvania, Philadelphia, Pennsylvania 19104*
[18] *University of Pittsburgh, Pittsburgh, PA 15260*
[19] *Istituto Nazionale di Fisica Nucleare, University and Scuola Normale Superiore of Pisa, I-56100 Pisa, Italy*
[20] *Purdue University, West Lafayette, Indiana 47907*
[21] *University of Rochester, Rochester, New York 15627*
[22] *Rockefeller University, New York, New York 10021*
[23] *Rutgers University, Piscataway, New Jersey 08854*
[24] *Texas A&M University, College Station, Texas 77843*
[25] *University of Tsukuba, Tsukuba, Ibaraki 305, Japan*
[26] *Tufts University, Medford, Massachusetts 02155*
[27] *University of Wisconsin, Madison, Wisconsin 53706*

Abstract

Kinematic properties of four-jet events produced in $p\bar{p}$ collisions at $\sqrt{s} = 1.8$ TeV have been studied using data with an integrated luminosity of 325 nb^{-1} collected using the Collider Detector at Fermilab (CDF) during the 1988-1989 Fermilab Collider run. The individual jet p_T spectra and the angles between each jet pair are compared to the predictions of leading order quantum chromodynamics for the double gluon bremsstrahlung process (DB) and good agreement is observed. In addition, a search for double parton (DP) scattering has been undertaken using variables sensitive to the topology of four-jet events. A small double parton content provides the best description of the data. We find $N_{\rm DP}/N_{\rm DB} = 5.4^{+1.6}_{-2.0}$ %, where N represents the number of events attributed to each process. We measure $\sigma_{\rm DP} = 63^{+32}_{-28}$ nb for jets having $p_T > 25$ GeV/c in the pseudorapidity interval $|\eta| < 3.5$.

I Introduction

In the context of the standard model, the dominant mechanism for the production of events containing four high transverse momentum (p_T) jets at the Tevatron is double gluon bremsstrahlung, as described by perturbative quantum chromodynamics (QCD). A small subset of the allowed Feynman diagrams (to leading order in α_s) is shown in Fig. 1. Expressions exist for all leading order diagrams [1], allowing a quantitative theoretical determination of the kinematics and topology of this complex process. In this article, we present the first comparison of high statistics data and QCD predictions for the double bremsstrahlung process at $\sqrt{s} = 1.8$ TeV.

In recent years, there has been considerable interest in the possibility of four-jet production through a "double parton scattering" mechanism [2]. This process, shown schematically in Fig. 2, involves *two* hard scatterings within one hadron-hadron collision. Naively,

the final state configuration can be described using a pair of dijet events, assuming that the collisions occurred independently. The interest in double parton scattering is motivated by the desire to measure parton correlations within hadrons [3]. Additionally, double parton scattering presents a background to any process leading to the production of four-jet events.

Due to the complexity of the process, theoretical guidance with regard to the double parton cross section ($\sigma_{\rm DP}$) is limited. One approach, which has been adopted in previous studies [4, 5], is that $\sigma_{\rm DP}$ is proportional to the dijet cross section, $\sigma_{\rm dijet}$, multiplied by the probability of a further dijet interaction. This can be expressed as follows:

$$\sigma_{\rm DP} = \sigma_{\rm dijet} \cdot \frac{\sigma_{\rm dijet}}{2\sigma_{\rm eff}} \tag{1}$$

where the effective cross section, $\sigma_{\rm eff}$ is introduced to represent the possible effects of parton correlations. If parton correlations are negligible, $2\sigma_{\rm eff}$ should approximately equal the total inelastic cross section of 44 mb [6]. The factor of two is typically included to account for Poisson statistics. This implies $\sigma_{\rm eff} \approx 22$ mb.

It is standard procedure [4, 5] to also include a correction for geometric effects. The occurrence of one hard scatter in a proton-antiproton collision preferentially selects configurations where the proton and antiproton have large overlap, thus increasing the probability of an additional hard scatter. The resulting enhancement factor is 2.3 [4] assuming the proton is an homogeneous hard sphere. This increase in the double parton cross section translates to a decrease in $\sigma_{\rm eff}$. Under these assumptions, we arrive at the approximate relation $\sigma_{\rm eff} \approx 10$ mb. One should bear in mind that parton correlations tend to reduce the effective cross section (i.e. increase the double parton scattering cross section) relative to the uncorrelated case [7].

To date, the results of two experimental searches for double parton scattering have been published. The Axial Field Spectrometer collaboration (AFS) found a significant

double parton signal in data taken at the ISR with $\sqrt{s} = 63$ GeV [4], and measured $\sigma_{\rm eff} \sim 5$ mb. For their study, jets with $p_T > 4$ GeV/c contained within the pseudorapidity interval $|\eta| < 1.0$ were used. The UA2 collaboration however, did not find evidence for the double parton process at $\sqrt{s} = 630$ GeV [5], and set the limit $\sigma_{\rm eff} > 8.3$ mb (95% C.L.) for jets having $p_T > 15$ GeV/c and $|\eta| < 2$.

Under the assumption that the double parton scattering cross section is proportional to the square of the dijet cross section, one expects $\sigma_{\rm DP} \propto f^4$, where f represents $f(x, Q^2)$, the parton distribution function. The corresponding dependence for the four-jet cross section from QCD double bremsstrahlung is $\sigma_{\rm DB} \propto f^2$. At constant momentum transfer Q^2, parton densities increase with decreasing Feynman x [8]. Therefore experiments operating at higher center-of-mass energies will produce a higher rate of double parton events relative to double bremsstrahlung events for a given minimum jet p_T requirement. Qualitatively then, the high center-of-mass energy available at the Tevatron collider provides strong motivation for our search for double parton scattering.

The paper is organized as follows: Section II gives a brief description of the detector components relevant to this analysis. Sections III and IV explain the measurement of jets at CDF and how we correct for detector effects such as calorimeter nonlinearity and uninstrumented regions. Section V describes the analysis cuts necessary in order to remove trigger bias and ensure data of good quality. In Section VI we perform a kinematical and topological comparison of four-jet data with QCD and phase space models. Section VII explains the procedure used to search for double parton interactions, and Section VIII describes our measurement of the double parton and effective cross sections. Section VIII also contains a discussion of the expected rate of double parton scattering at the SSC. Conclusions from this work are presented in Section IX.

II Detector

Since the CDF detector has been described in detail elsewhere [9], only a brief description of those components relevant to this analysis will be given. The CDF coordinate system is defined with the z axis along the proton direction, and the polar angle θ is measured with respect to this axis. The azimuthal angle around the beam axis is denoted by ϕ. We define "detector pseudorapidity" η_d, which differs from the event frame pseudorapidity η, as pseudorapidity measured from the center of the detector (z=0). This variable is of use particularly in the context of our jet correction (see Sec. IV) which is a function of position within the detector.

Electromagnetic (em) and hadronic (had) calorimeters cover the full range of azimuth in the range $\mid \eta_d \mid < 4.2$. They are segmented into projective towers pointing towards the center of the detector. The calorimeters occupying the region $\mid \eta_d \mid < 1.1$ are scintillator-based, with the tower segmentation $\Delta\eta_d = 0.1$ and $\Delta\phi = 15°$. In the region $1.1 < \mid \eta_d \mid < 4.2$ multiwire proportional gas chambers are used, with a finer azimuthal segmentation, $\Delta\phi = 5°$.

The event vertex was reconstructed using a vertex time projection chamber system (VTPC) [10] that surrounded the beam pipe. The vertex position in the z direction (z_{vert}) was observed to have a Gaussian shape with $\sigma = 30$ cm, centered at z = 0 cm. The VTPC was also used to reject events with more than one event vertex, where the two vertices were separated by more than 5 cm. The jet pseudorapidities were measured with respect to the event vertex rather than the center of the detector.

A Trigger

The CDF trigger was arranged into four levels [11]. The level 0 trigger required hits in both forward and backward scintillation (beam-beam) counters within a 15 ns window centered

on the beam crossing time. The cross section for this trigger was 47±3 mb [6], which corresponds to an event rate of 47 kHz at the typical Tevatron luminosity of 10^{30} cm^{-2}s^{-1}. This rate was reduced to 1-2 Hz by the three subsequent trigger levels.

In the trigger, calorimeter towers were merged to produce a segmentation of $\Delta\phi = 15^\circ$ and $\Delta\eta_d = 0.2$. The level 1 stage of the jet triggers required that the total scalar transverse energy (E_T) for all trigger towers having $E_T > 1$ GeV be greater than 18 GeV. The level 2 stage performed jet clustering by taking trigger towers with $E_T > 3$ GeV and merging them with contiguous trigger towers having $E_T > 1$ GeV. For this study, a special multijet trigger was implemented. It required:

(i) At least 2 clusters ($E_T \geq 3$ GeV for each cluster). The transverse energies of the two largest clusters we label E_{T_1} and E_{T_2}.

(ii) $\sum E_T > 80$ GeV over the entire calorimeter, where the sum includes towers with $E_T \geq 1$ GeV in either the electromagnetic or hadronic calorimeters.

(iii) $\sum E_T - E_{T_1} - E_{T_2} > 40$ GeV.

The last requirement was used to reject dijet events, and will henceforth be known as the level 2 dijet veto cut.

The level 3 stage of the multijet trigger [12] used fully reconstructed calorimeter information. Jets were clustered using the standard CDF algorithm [13] and four jets were required with $p_T > 15$ GeV/c in the pseudorapidity interval $|\eta_d| < 4.2$. The event z vertex position was assumed to be located at $z_{\rm vert} = 0$ cm, and jets were not corrected for detector mismeasurement. The effect on the data of these trigger requirements will be treated in Sec. V. Approximately 33,000 events passed these requirements from a total integrated luminosity of 325 nb^{-1}.

III Jet Clustering Algorithm

Jet clustering at CDF is performed using a fixed cone algorithm and is described in detail in Ref. [13]. The fixed cone algorithm corresponds closely to definitions used in calculating QCD cross sections [14, 15, 16]. The jet cone size R used in this analysis is given by

$$R = \sqrt{(\Delta\eta)^2 + (\Delta\phi)^2} = 0.7. \tag{2}$$

Studies have shown that any cone size in the interval 0.4–1.0 includes a major fraction of jet energy and hence is suitable for jet identification [13].

The properties of clustered jets were obtained from the electromagnetic and hadronic calorimeter towers contained within the clustering cone of size $R = 0.7$. Only towers with transverse energy greater than 100 MeV were included. The relevant jet quantities are defined as follows:

$$p_x = \sum_i (E^i_{em} + E^i_{had}) \sin\theta^i \cos\phi^i, \tag{3}$$

$$p_y = \sum_i (E^i_{em} + E^i_{had}) \sin\theta^i \sin\phi^i, \tag{4}$$

$$p_T = \sqrt{p_x^2 + p_y^2}, \tag{5}$$

$$E = \sum_i (E^i_{em} + E^i_{had}), \tag{6}$$

$$E_T = E\frac{p_T}{|\vec{p}|}, \tag{7}$$

where θ is the polar angle of the tower, corrected for the position of the event vertex. The jet position in η-ϕ space was determined using the cluster E_T-weighted center-of-mass.

IV Jet energy corrections

In our study of four-jet events we investigated the p_T balancing of dijet pairs within the events. It was therefore necessary to correct the jet energies for detector effects (i.e. unin-

strumented areas, nonlinearity of the energy measurement) which could affect this balancing [17]. The correction was performed in two stages.

A Relative correction

A correction for the variation in CDF calorimeter response as a function of η_d was applied in the form of a multiplicative factor, dependent on both jet p_T and η_d. This factor corrects the p_T of a jet anywhere in the calorimeter to the equivalent p_T that would be measured in the region $0.2 <\mid \eta_d \mid < 0.7$ (henceforth referred to as the "central" region). We chose to correct all jets to the central region since measurements there were performed using scintillator-based calorimeters with superior resolution [18]. We avoided the regions $\mid \eta_d \mid < 0.2$ and $\mid \eta_d \mid > 0.7$ since jets in these regions are affected by the boundaries between calorimeter components.

The relative jet correction function was constructed using dijet events collected with single jet triggers having level-3 cluster thresholds of $E_T > 20$, 40 and 60 GeV. A cut on the scalar $\sum p_T$ of both jets was placed in order to remove trigger bias, and at least one jet was required to be located within the central region. For ease of reference, we refer to the jet in the central region as the "trigger" jet, and the remaining jet as the "probe" jet. Jets in this sample should, on average, balance in $\vec{p_T}$. A systematic $\vec{p_T}$ imbalance in the calorimeter indicates an energy scale difference between the central region and the probe jet region. In an event, the dijet system can have a small transverse boost, as a result of soft gluon radiation, which is balanced by unclustered transverse energy. This boost will tend to broaden the dijet p_T balancing distribution. For improved balancing resolution, we utilize missing E_T ($\vec{\not\!\!E}_T$) instead of dijet $\vec{p_T}$ imbalance. We calculate $\vec{\not\!\!E}_T$ by summing calorimeter energy cells with $E_T > 100$ MeV:

$$\vec{\not\!\!E}_T = -\sum_i E_T^i \hat{n}_i, \tag{8}$$

where $\hat{n}_i$ is a unit vector perpendicular to the beam axis and pointing at the ith tower. The sum is over all cells with $\mid \eta_d \mid < 3.6$. We then form the $\vec{\not\!\!E}$ projection fraction (h)

$$h = \frac{2 \cdot \vec{\not\!\!E}_T \cdot \hat{p}_T^{\rm probe}}{p_T^{\rm trigger} + p_T^{\rm probe}}, \tag{9}$$

where $p_T^{\rm trigger}$ and $p_T^{\rm probe}$ are the scalar transverse momenta of the trigger and probe jets respectively, and $\hat{p}_T^{\rm probe}$ is a unit vector in the transverse plane defined by the direction of the probe jet. Figure 3a) shows h as a function of η_d for dijet data in the range $50 < \sum p_T < 100$ GeV/c. There is a pronounced variation, particularly at calorimeter boundaries ($\mid \eta_d \mid \sim$ 0, 1.1 and 2.2). Using the average h in each bin of η_d, we derive the correction factor, $\beta_R = < p_T^{\rm trigger}/p_T^{\rm probe} >$; the effect of the transverse boost cancels in the average. We determine β_R as a function of η_d for five $\sum p_T$ bins, 50–100, 100–130, 130–170, 170–200 and $>$ 200 GeV/c. In forming the correction function, the variation of β_R with η_d was parametrized with a cubic spline, and the dependence on p_T was parametrized linearly. As a consistency check, the correction was applied to the dijet data, and the h variable formed again after adjusting $\vec{\not\!\!E}_T$ for the difference between corrected and uncorrected jet p_T. The corrected distributions of h were flat as a function of η_d at the level of a few per cent for each of the five ranges of $\sum p_T$. Figure 3b) shows the corrected distribution for the dijet data in the range $50 < \sum p_T < 100$ GeV/c.

B Absolute correction

The goal of the absolute jet energy correction is to correct for effects such as the nonlinear response of the hadron calorimeter. The correction algorithm was derived using Monte Carlo simulations of both the fragmentation process and the CDF detector.

Jet events were generated in the central pseudorapidity region with a flat p_T spectrum. Fragmentation was performed using a Feynman-Field parametrization [19, 20], and

the resulting particles were passed to the detector simulation. The response of the central hadron calorimeter as measured using a test beam and *in situ* [13] was incorporated in the simulation. An "underlying event" was also generated (see Sec. C). Jets were clustered using the standard CDF algorithm. Cluster p_T was compared to the magnitude of the vector sum of all particles whose initial direction was contained within the corresponding jet cone, $p_T^{\rm cor}$. In the region of jet p_T relevant to this analysis ($25 < p_T^{\rm cor} < 150$ GeV/c) the results were well described by the relation:

$$p_T^{\rm cor}({\rm GeV/c}) = 2.1 + 1.2 \cdot p_T^{\rm cluster} - 0.0008 \cdot (p_T^{\rm cluster})^2, \qquad (10)$$

where $p_T^{\rm cluster}$ refers to the p_T measured using the central calorimeter for a cone radius of $R = 0.7$. This function defines the absolute jet p_T correction. The uncertainty on the jet absolute p_T scale in the central region is approximately $\pm 5\%$ in the corrected p_T range $25 < p_T^{\rm cor} < 150$ GeV/c [21].

C Underlying event and clustering corrections

The term "underlying event" refers to a collection of relatively low p_T particles arising from interactions between spectator partons. These particles can contribute a small amount of additional energy to the jet cone. Underlying event energy deposition has been studied with data collected using only the level 0 trigger ("minimum bias" data). For a cone radius of 0.7, an average E_T of approximately 1 GeV (corrected) is contributed.

The nature of the fragmentation process generally results in some fraction of the fragmentation products falling outside the clustering cone. Using the same Monte Carlo programs discussed in Sec. B, the magnitude of the vector sum p_T of particles falling outside a cone of 0.7 was determined. This quantity will be referred to as out-of-cone p_T (or $p_T^{\rm out}$). The initial direction of the particle $\vec{p_T}$ (before propagation through the magnetic field which

exists in the central region) was used to decide whether the particle should be classified as inside or outside the cone. Using our fragmentation model, $p_T^{\rm out}$ was observed to increase slowly as a function of $p_T^{\rm cor}$. This behaviour was parametrized using the form

$$p_T^{\rm out} = \alpha(1 - \beta e^{-\gamma p_T^{\rm cor}}). \tag{11}$$

For a cone size $R = 0.7$, we found $\alpha = 8.4$ GeV/c, $\beta = 0.85$ and $\gamma = 0.0073$ $(\text{GeV/c})^{-1}$. Using this parametrization, the ratio of $p_T^{\rm out}$ to $p_T^{\rm cor}$ as a function of $p_T^{\rm cor}$ is shown in Fig. 4. Also shown is the ratio of underlying event p_T to $p_T^{\rm cor}$, which is a significantly smaller effect. In our analysis we make no correction for underlying event energy, or energy lost outside the clustering cone, since such corrections are strongly model dependent. Instead, we take these effects into account by including them in our estimation of jet energy scale uncertainty (see Sec VIIIA).

V Analysis

Events were selected from the data sample by applying the following cuts:

(i) $\mid z_{\rm vert} \mid < 60$ cm.

(ii) Four jets with $p_T > 25$ GeV/c after correction.

(iii) Jet $\mid \eta_d \mid < 3.5$.

(iv) Jet axis separation > 1.0 in the η-ϕ metric.

(v) No second event vertex.

(vi) $\Sigma p_T > 140$ GeV/c (scalar sum over the leading four jets).

These cuts will henceforth be referred to as the *standard* data analysis cuts. The effect of these cuts on the total number of events in the sample is shown in Table 1. The cut on the vertex position along the z axis, $\mid z_{\rm vert} \mid < 60$ cm, was necessary to avoid distortion of the projective calorimeter tower geometry. The single jet cut $p_T > 25$ GeV/c was imposed

in order to remove bias introduced by the level 3 trigger. It should be noted that this trigger passed clusters with uncorrected $p_T > 15$ GeV/c assuming a vertex located at $z_{vert} = 0$ cm. After applying the jet p_T and event vertex corrections, the corrected p_T of a cluster having $p_T = 15$ GeV/c may be greater than 20 GeV/c. This effect was studied in detail using a simulation of the level 3 trigger. We found that 98% of jets passing a cut of $p_T > 25$ GeV/c (corrected) would have passed the trigger requirement of $p_T > 15$ GeV/c (uncorrected).

We imposed the condition $| \eta_d | < 3.5$ on all jets so that they were completely contained within the calorimeter. The cut on the corrected scalar sum p_T of the four jets, $\sum p_T > 140$ GeV/c, removed trigger bias introduced by the level 2 ΣE_T trigger which required $\Sigma E_T > 80$ GeV. This cut was determined to be fully efficient (see Sec.VI). The level 2 ΣE_T for data and simulation were in good agreement, as shown in Fig. 5.

In order to obtain smooth Monte Carlo distributions with limited computing resources, a fast parton level detector simulation was used for much of the analysis. This simulation reproduced global jet quantities such as p_T, η and ϕ without the intermediate steps of fragmentation and clustering. The relative and absolute jet energy corrections were incorporated in reverse, and jet p_T and position resolutions were tuned to agree with dijet data.

In the regions where jets are completely contained within one calorimeter system, the jet p_T resolution is well modeled by the relation [22]

$$\sigma(p_T) = 0.1 \cdot p_T + 1.0 \text{ (GeV/c)}. \tag{12}$$

In the crack regions of the calorimeter ($| \eta_d | \sim 0$, 1.1 and 2.2) the resolution is approximately 10% worse. The difference between the jet p_T resolutions determined using data and the fast jet simulation (which used the parametrization given in Eq. 12) was found to be less than 20% in all regions of the calorimeter [17]. To check the effect of jet resolution uncertainty

on the results contained in this analysis we varied the resolution by $\pm 20\%$. No significant effect on the simulated distributions was observed.

VI QCD Comparison

Double bremsstrahlung events at the parton level were simulated using the approximate matrix element of Kunszt and Stirling [23] provided in the PAPAGENO computer program [24]. We chose our default structure function to be Morfin and Tung set 1 (DIS) [25] with a default renormalization scale $Q = \langle p_T \rangle$. We also generated parton distributions using a uniform matrix element (four-body phase space) in place of the QCD four-jet approximation. In order to model the effects of additional gluon radiation (fifth jets) we applied a small transverse Lorentz boost ("k_T kick") to the four-jet system. The magnitude of the kick, distributed as a Gaussian of width approximately 5 GeV/c, was determined using dijet data. The fast jet simulation was used to model detector effects; the resulting jets were then corrected (as described in Sec. IV) and the standard analysis cuts were applied.

For the purposes of avoiding the singularities inherent in the matrix element calculation and increasing generation efficiency, the following cuts were placed on partons generated with the double bremsstrahlung simulation:

(i) $p_T > 13$ GeV/c.

(ii) Parton separation $| \Delta R | > 0.8$.

(iii) $| \eta_d | < 4.0$.

Shown in Fig. 6 are distributions of parton p_T, separation and η_d of the lowest and highest p_T jets after applying the standard cuts and corrections.

A comparison of the p_T spectra between data, QCD and phase space for each of the four jets has been performed. Before comparison, the jets were ordered in p_T; jet 1 having the largest p_T after correction, jet 2 the next largest and so on. Also, we have formed the

scalar sum p_T (after correction) of all four jets. The results are shown in Figs. 7 and 8 where the QCD and phase space distributions have been normalized to have the same area as the data. The QCD and phase space predictions are very similar for these distributions, and the data points are well described by both. The normalization factor for the double bremsstrahlung Monte Carlo distributions was approximately 1.5 (using structure function Morfin-Tung set 1 (DIS) with $Q = \langle p_T \rangle$). This difference between measured and predicted rates is well within experimental and theoretical uncertainties.

To describe the topology of the four-jet system, nine variables are needed. Three of these were used to boost the system to the center-of-mass reference frame. The six remaining degrees of freedom were associated with the six independent interjet angles. In the center-of-mass frame we define the angle between jets i and j as Ω_{ij} and use the variables $\cos\Omega_{ij}$ in order to make a comparison. Here ij is one combination from the six possible choices (12,13,14,23,24,34) where jets have been ordered in p_T as described above. The results for the data, together with the QCD four-jet prediction and the phase space results, are shown in Fig. 9 where all distributions have been normalized to unit area.

In all six cases, good agreement between the data and QCD is observed. The angular distributions obtained with a phase space generator are quite different from the QCD results. Similar effects have been observed in events containing three or more energetic jets [13]. The level of agreement found in both the p_T spectra and angular distributions is insensitive to changes in either the structure function or renormalization scale used in the QCD double bremsstrahlung simulation.

VII Double Parton Analysis

In order to perform a Monte Carlo calculation of the relative rates for double parton and double bremsstrahlung events, we assumed a value $\sigma_{\rm eff} = 10$ mb, as discussed in the intro-

duction. Our double parton simulation was constructed by merging two dijet events at the parton level. Each dijet system was independently given a small transverse k_T kick. As constructed, our double parton model operates under the assumption that parton correlations are negligible.

The Monte Carlo cross sections for both double parton and double bremsstrahlung processes at the parton level are shown in Fig. 10 a) and b) as a function of minimum jet p_T, and jet scalar Σp_T respectively. These figures indicate that the double parton signal will be small for a minimum p_T above 20 GeV/c. Note that the absolute values of both theoretical cross sections vary by approximately a factor of two, depending on the choice of structure function and renormalization scale.

A Method

The key ingredient in our search for double parton scattering is the construction of topological variables which have a significant difference in shape for signal (double parton) and background (double bremsstrahlung). We have used two such variables.

The first variable, S, exploits the tendency of jets produced by double parton scattering to balance pairwise in p_T [26], and is defined as:

$$S(i+j,k+l) \equiv \sqrt{\left[\left(\frac{|\vec{p_{T_i}}+\vec{p_{T_j}}|}{\sqrt{p_{T_i}+p_{T_j}}}\right)^2+\left(\frac{|\vec{p_{T_k}}+\vec{p_{T_l}}|}{\sqrt{p_{T_k}+p_{T_l}}}\right)^2\right]/2}, \tag{13}$$

where S is minimized over the three possible jet pairings $(12,34)$, $(13,24)$ and $(14,23)$. On average, S will be smaller for double parton events than for double bremsstrahlung events. The shapes of S for both processes are shown in Fig. 11a).

Having defined a variable which depends on jet p_T, a separate variable may be constructed which takes advantage of the differences in *angular* correlations between jets produced by the two mechanisms[3]. We define ϕ_{ij} to be the azimuthal angle of the vector

$\vec{p}_{Ti} + \vec{p}_{Tj}$, where i and j refer to two separate jets. Jets are first arranged into two pairs according to the configuration which minimizes S. Assuming that this results in the pairing (ij, kl), we then define Δ_S as the angle between ϕ_{ij} and ϕ_{kl}. The Δ_S variable spans the interval 0–π, and is shown for Monte Carlo double parton and double bremsstrahlung four-jet events in Fig. 11b).

An example of how the Δ_S variable is calculated is shown in Fig. 12 for a typical double bremsstrahlung and double parton event in the transverse plane. The dynamics of double gluon bremsstrahlung are such that configurations where the gluons are emitted close to the original parton direction are preferred (see Fig. 9). Combined with our ordering procedure, this gives a distribution which peaks at $\Delta_S = \pi$. For real jets in the detector, this distribution is smeared by effects such as additional soft gluon radiation and detector resolution.

In the simple model of double parton scattering, partons exactly balance pairwise in $\vec{p}_T$, and Δ_S is therefore not defined. However, as in the case of double bremsstrahlung events, jets in the detector resulting from these partons will *not* balance exactly. Assuming no parton correlations, the azimuthal angles of the resultant jet pairwise p_T vectors (after pairing to minimize S) should be randomly distributed, and thus uniformly distributed in the range $0 - \pi$.

Using simulations of both the double parton and double bremsstrahlung processes, a quantitative analysis of the respective signal-finding abilities of the S and Δ_S variables was performed. Parton level events were passed to the fast detector simulation, then the jet corrections and analysis cuts were applied. A Monte Carlo sample was constructed, consisting of 10% double parton and 90% double bremsstrahlung events. This sample was fitted to a normalized admixture of signal and background shapes and the χ^2 per degree of freedom, χ^2_r, was evaluated using Poisson statistics. The behaviour of χ^2_r as a function of

double parton content provides a measure of the signal-finding resolution of each variable. The result of this study, shown in Fig. 13, reveals that the Δ_S variable is slightly more effective than S.

The effect of additional gluon radiation on the S and Δ_S distributions must also be evaluated. If the additional gluon radiation is at high enough p_T, it can result in the formation of an additional cluster. At low p_T it may simply introduce a transverse boost (k_T kick) to the four-jet system, possibly disrupting the pairwise $\vec{p}_T$ balancing and jet pair angular distributions. Recall that our double bremsstrahlung simulation includes a k_T kick, but that this kick was tuned using dijet data. The ability of our double bremsstrahlung simulation to model fifth jet effects was tested qualitatively using a Monte Carlo simulation of five-jet events, where only four jets passed the standard analysis cuts. Five-jet events were generated according to the gluon scattering matrix element $gg \rightarrow ggggg$. The distributions obtained are shown in Fig. 14. The effect of a fifth jet is to create a *depletion* in the signal region for S, and an *enhancement* in the signal region for Δ_S.

In order to investigate the effect of a k_T kick or fifth clusters in more detail, we plot the missing p_T calculated from the vector sum of the four leading jets. Figure 15 shows the data compared to the four-jet Monte Carlo sample. The distributions disagree ($\chi^2_r \approx 6$) when a large fifth jet is allowed. However, when the maximum p_T of the fifth jet is required to be below 15 GeV, good agreement ($\chi^2_r \approx 1$) between the data and the Monte Carlo is observed. The Monte Carlo and data begin to diverge if the cut on the fifth jet p_T is reduced below approximately 10 GeV/c. This is because the 4-jet Monte Carlo contains a k_T kick which models the effect of low p_T fifth jets without actually producing an additional cluster. By making a very tight cut on fifth jet p_T we are removing events with a large k_T kick from the data but not from the Monte Carlo sample. We therefore conclude that our double bremsstrahlung model is correctly simulating the effects of additional gluon radiation when

a cut on fifth jets in the data is imposed in the range 10–15 GeV/c.

The four-jet data were fit to an admixture of simulated double parton and double bremsstrahlung distributions using both the S and Δ_S variables. The only free parameter was the relative fraction of each process $\mathcal{R}$, defined as

$$\mathcal{R} = \frac{N_{\rm DP}}{N_{\rm DB}}, \tag{14}$$

where $N_{\rm DP}$ and $N_{\rm DB}$ represent the number of double parton and double bremsstrahlung events respectively. The results are shown in Figs. 16 a) and b) for the case where a fifth jet cut of 15 GeV has been applied to the data. The fitted values of $\mathcal{R}$ for S and Δ_S agree within statistical uncertainties. The respective signal regions for S and Δ_S are indicated by arrows. The behaviour of $\mathcal{R}$ in response to a range of cuts on p_{T5} for both variables can be seen in Fig. 17. As expected from the study of the effect of fifth jets and k_T kick, the S and Δ_S measurements give different results when large fifth jets are allowed in the data (fifth jets create a *depletion* in the signal region for S, and an *enhancement* in the signal region for Δ_S). The results using S and Δ_S are in good agreement for a fifth jet p_T cut in the range 10–15 GeV/c. This is consistent with the results of our missing p_T study.

In order to determine $\mathcal{R}$ and its corresponding uncertainty, we adopt the following procedure. First, a straight line is fit to S and Δ_S versus maximum p_{T5} (or $p_T^{\rm max}$), as shown in Fig. 17. The point of intersection of these lines determines $\mathcal{R}$, and the value of $p_{T5}^{\rm max}$ at this point we label p'_{T5}. Making the cut $p_{T5} < p'_{T5}$, we then perform a *combined* fit to S and Δ_S using an admixture of signal and background shapes. The statistical uncertainty on $\mathcal{R}$ is then taken to be the change in $\mathcal{R}$ necessary to increase the fit χ^2 (evaluated using Poisson statistics) by 1 unit. This method is chosen since it takes into account the effect of correlations between the two variables. The systematic uncertainty on $\mathcal{R}$ arising from the cut on p_{T5} is determined as follows:

(a) Construct error bounds of $\pm 1\sigma$ on the straight line fits to S and Δ_S versus $p_{T5}^{\max}$ (as shown in Fig. 17).

(b) Determine $p_{T5}^{\max}$ at the right- and left-most intersection of the S and Δ_S error bounds ($p_{T5}^{\max} \approx 15$ GeV/c and $p_{T5}^{\max} \approx 10$ GeV/c, respectively). This also represents the range of fifth jet p_T cuts for which we have confidence in the k_T kick modeling of fifth jet effects.

(c) Find the two corresponding values of $\mathcal{R}$ for the two values of $p_{T5}^{\max}$ found in (b). The range covered by these values is representative of the systematic uncertainty on $\mathcal{R}$ due to the cut on fifth jets and our modeling of the k_T kick in the Monte Carlo.

The result obtained using structure function Morfin-Tung DIS set 1 with $Q = \langle p_T \rangle$ for both double bremsstrahlung and double parton simulations is

$$\mathcal{R} = 0.054 \pm 0.013 \text{ (stat.)}^{+0.010}_{-0.015} \text{ (syst.)}. \tag{15}$$

Combining systematic and statistical uncertainties in quadrature, we find

$$\mathcal{R} = 0.054^{+0.016}_{-0.020}. \tag{16}$$

Additional sources of systematic uncertainty on $\mathcal{R}$ were investigated. There was no significant change in $\mathcal{R}$ when either the structure function or momentum scale used in the QCD simulations were changed. We also observed no change in $\mathcal{R}$ when a different four-jet matrix element approximation was used [27]. The level 2 dijet veto cut (defined in Sec. IIA) was studied in detail in order to determine its effect on S and Δ_S. This trigger cut was found not to bias either of the variables, and hence was not a source of uncertainty on $\mathcal{R}$. Thus, the double parton signal is significant at the 2.7σ level.

B Double interactions

As a result of the luminosity conditions of the 1988/89 run ($\mathcal{L}(\text{peak}) \sim 2 \times 10^{30}$ cm^{-2}s^{-1}), combined with the trigger biases, approximately 20% of events taken with the multijet

trigger contained two separate $p\bar{p}$ interactions. If both interactions produce dijets, then the resulting event topology will mimic that of the double parton process. We rejected approximately 85% of events containing two interactions using the VTPC [6]. The remaining 15% could not be rejected because the two interactions occurred close together, and were therefore not resolved. After the VTPC cut, approximately 3% ($= 15\% \times 20\%$) of events in the four-jet sample contain an unresolved secondary interaction.

In order to determine the nature of the events containing an unresolved secondary vertex we performed a Monte Carlo study of the relative rates of the two dominant channels leading to a four-jet final state. These channels are a) two dijet pairs (the potential background) and b) a combination of one double bremsstrahlung event and one minimum bias event. Using the standard analysis cuts we found that the number of double dijet events produced via double interactions was approximately a factor of 20 smaller than the number of double bremsstrahlung plus minimum bias events [17]. This conclusion was checked experimentally by examining the S distribution for events containing two resolved event vertices in the four-jet data. These events satisfied all the standard analysis cuts with the exception of the cut on secondary vertices. The shape of S using these events was consistent with that formed using events which passed all the standard analysis cuts, and which were mainly produced via double bremsstrahlung. We conclude that the production of two dijet pairs from double interactions is a negligible background to the double parton process for our event sample.

VIII Measurement of $\sigma_{\rm DP}$ and $\sigma_{\rm eff}$

A Determination of $\sigma_{\rm DP}$

The double parton cross section for the standard cuts can be expressed as

$$\sigma_{\rm DP} = \frac{N_{\rm DP}}{\mathcal{L} \cdot \mathcal{A}_{\rm DP}^{\rm cuts} \cdot \mathcal{A}_{\rm DP}^{\rm trig}}, \tag{17}$$

where $\mathcal{L}$ is the integrated luminosity of the event sample, $\mathcal{A}_{\rm DP}^{\rm cuts}$ is the acceptance of the four-jet event cuts, and $\mathcal{A}_{\rm DP}^{\rm trig}$ is the acceptance of the multijet trigger for double parton events. Values and corresponding uncertainties for the terms in Eq. 17 are given in Table 2. We also include in this table a value for the dijet cross section $\sigma_{\rm dijet}$ (see Sec. B) which is necessary in order to evaluate $\sigma_{\rm eff}$.

Double parton events were generated with parton $p_T > 18$ GeV/c. No partons below this p_T pass the standard analysis cut $p_T > 25$ GeV/c (corrected). Therefore our measurement of $\sigma_{\rm DP}$ refers to the cross section for partons with $p_T > 18$ GeV/c. The integrated luminosity of the event sample was determined to be [6]

$$\mathcal{L} = 325 \text{ nb}^{-1} \pm 7\%. \tag{18}$$

This luminosity was less than the total integrated luminosity for the 1988/89 run ($\sim$4 pb^{-1}) because a) the trigger was prescaled by a factor of 100 during periods of high luminosity and b) the trigger was only in use for 3 out of the total 12 months of data-taking.

The acceptance of the standard event cuts for double parton events ($\mathcal{A}_{\rm DP}^{\rm cuts}$) was calculated using the double parton simulation, in conjunction with the fast jet Monte Carlo program. We find [17]

$$\mathcal{A}_{\rm DP}^{\rm cuts} = (6.5 \pm 0.9) \times 10^{-3} \ \ (\text{parton } p_T > 18 \text{ GeV/c}). \tag{19}$$

This acceptance is small because the analysis cuts only become fully efficient for parton $p_T \sim 30$ GeV/c, and we include all partons with $p_T > 18$ GeV/c. The quoted systematic uncertainty on $\mathcal{A}_{\rm DP}^{\rm cuts}$ stems from renormalization scale and structure function uncertainty (the latter being particularly large for partons with low Feynman x). The acceptance of the standard event cuts was re-evaluated using various different structure functions. We used MRS sets 1, 2 and 3, and DFLM [28] sets 1, 2 and 3 for this purpose. Also, we used both

$Q = \langle p_T \rangle$ and $Q = \langle p_T/2 \rangle$ in order to estimate the uncertainty associated with the choice of the renormalization scale used in the QCD calculation. The acceptance and uncertainty quoted in Equation 19 are the mean and standard deviation of the results obtained using the structure functions and renormalization scales mentioned above. The effect on $\mathcal{A}_{\rm DP}^{\rm cuts}$ of jet resolution uncertainty (as modeled by the fast jet simulation) was negligible. The effect of jet energy scale uncertainty is discussed below, since it also affects $N_{\rm DP}$ and hence enters into the uncertainty on $\sigma_{\rm DP}$ as a ratio.

The acceptance of the trigger for double parton events was determined using a sample of double parton events with full detector and trigger simulations. The biggest loss in acceptance resulted from the level 2 dijet veto cut (defined in Sec. IIA). The standard analysis cuts ensured almost complete acceptance for the level 2 cut $\Sigma E_T > 80$ GeV and the level 3 cut jet $p_T > 15$ GeV/c (uncorrected). We find [17]

$$\mathcal{A}_{\rm DP}^{\rm trig} = 0.85 \pm 0.10. \tag{20}$$

Defining $N_{\rm tot}$ as the total number of four-jet events in the data sample, the number of double parton events in the data, $N_{\rm DP}$, can be expressed as

$$N_{\rm DP} = N_{\rm tot} \left(\frac{\mathcal{R}}{1+\mathcal{R}} \right). \tag{21}$$

For the four-jet sample, $N_{\rm tot} = 2213$, and using the results of Eq. 16 for $\mathcal{R}$ we find $N_{\rm DP} = 113^{+34}_{-42}$. The uncertainty on $N_{\rm DP}$ quoted at this stage includes the uncertainty on $\mathcal{R}$ only.

A significant source of uncertainty on $\sigma_{\rm DP}$ is associated with jet energy scale uncertainty, which affects both $N_{\rm DP}$ and $\mathcal{A}_{\rm DP}^{\rm cuts}$. The following checks were made in order to evaluate the effect of jet energy scale uncertainty on $\sigma_{\rm DP}$:

(i) The absolute jet energy scale was raised and lowered by 5%.

(ii) The relative jet energy scale was increased and decreased by 2%. The relative scale in the central region ($0.2 <| \eta_d |< 0.7$) was not altered.

(iii) A correction was performed for underlying event energy inside the clustering cone.

(iv) A correction was performed for energy lost outside the clustering cone.

The resulting change in the ratio $N_{\rm DP}/\mathcal{A}_{\rm DP}^{\rm cuts}$ was found to be +20% and -26%.

In order to determine the final uncertainty on $\sigma_{\rm DP}$ a numerical technique was used. The quantities shown in Eq. 17 were simulated using Gaussian distributions with mean and standard deviation as measured. Where the uncertainties were not symmetric (e.g. jet energy scale uncertainty) we adopted the largest uncertainty. Then the distribution of $\sigma_{\rm DP}$ was formed, and the values of $\sigma_{\rm DP}$ on either side of the mean value containing $\pm 34.2\%$ of the total area were determined. Using this method, we obtain

$$\sigma_{\rm DP} = 63^{+32}_{-28}\ {\rm nb} \qquad ({\rm parton}\ p_T > 18\ {\rm GeV/c}). \tag{22}$$

B Determination of $\sigma_{\rm eff}$

In order to facilitate the comparison of our result with the results of other experiments, the effective cross section $\sigma_{\rm eff}$ was also determined. We calculated $\sigma_{\rm eff}$ using the result given in Eq. 22 for $\sigma_{\rm DP}$ combined with a determination of the dijet cross section for partons with $p_T > 18$ GeV/c. A leading order theoretical calculation was used, with the following result:

$$\sigma_{\rm dijet} = 39\ \mu{\rm b} \pm 20\% \quad ({\rm parton}\ p_T > 18\ {\rm GeV/c}). \tag{23}$$

This result reflects the average and standard deviation of results obtained using structure functions Morfin-Tung set 1 (DIS), MRS sets 1,2 and 3 and DFLM sets 1,2 and 3. For each structure function two different renormalization scales were used, $Q = \langle p_T \rangle$ and $Q = \langle p_T/2 \rangle$.

Combining uncertainties numerically using the technique described in Sec. A, we find

$$\sigma_{\rm eff} = 12.1^{+10.7}_{-5.4}\ {\rm mb}. \tag{24}$$

At the 95% confidence level, we obtain the following bounds on $\sigma_{\rm eff}$:

$$4.1 < \sigma_{\rm eff} < 41\ {\rm mb}\ (95\%\ {\rm C.L.}). \tag{25}$$

The fairly high upper limit is a result of the non-Gaussian shape of $\sigma_{\rm eff}$. Relaxing the confidence level to 90% we obtain:

$$5.4 < \sigma_{\rm eff} < 29\ {\rm mb}. \tag{26}$$

This result can be compared to those obtained by the AFS and UA2 collaborations. The AFS collaboration found a sizeable signal [4], and measured $\sigma_{\rm eff} \sim 5$ mb. The form for $\sigma_{\rm DP}$ used in their analysis was slightly different from the one used here. They also used the technique of merging dijet events, but the available energy for the second interaction was reduced, dependent upon the energy of the first interaction. This reduced the value of $\sigma_{\rm eff}$ by a factor of approximately 2 relative to the case where the second dijet event occurred at the same $\sqrt{s}$ as the first. They also included a K-factor in order to accommodate the effect of higher order corrections to the dijet cross section. In addition, the leading order double bremsstrahlung matrix element calculation was not available at the time this analysis was performed, and as a result a phenomenological model was used. The range of p_T and pseudorapidity used in the AFS analysis ($p_T > 4$ GeV/c, $\mid \eta \mid < 1.0$) was considerably different from that used in our study, as was the available center of mass energy ($\sqrt{s} =$ 63 GeV). In light of the significant differences between the two analyses, we cannot make a definitive statement about the consistency or inconsistency of these results.

The UA2 collaboration found no double parton signal, and set the limit $\sigma_{\rm eff} > 8.3$ mb (95% C.L.) at $\sqrt{s} = 630$ GeV. The p_T and pseudorapidity range of jets included in their

study ($p_T > 15$ GeV/c, $|\eta| < 2.0$) were similar to those used by CDF ($p_T > 25$ GeV/c, $|\eta| < 3.5$ GeV/c). We find that the results are consistent. In Table 3 we provide a summary of the experimental information on double parton scattering obtained using hadron colliders.

C Implications for the SSC

In order to investigate the implications of our result for physics at the SSC, a parton level Monte Carlo calculation was performed using $\sqrt{s}$=40 TeV for both double parton and double bremsstrahlung processes. We used $\sigma_{\rm eff} = 12.1$ mb in our double parton simulation. The chosen structure function and renormalization scale was Morfin-Tung set 1 (DIS) with $Q = \langle p_T \rangle$. Cross sections as a function of the p_T of the softest jet (p_{T4}) are shown in Figure 18. Based on this study, we expect a significant double parton signal at the SSC for jets with a minimum p_T cut-off below approximately 60 GeV/c. In fact, the double parton mechanism apparently dominates in the range $p_{T4} < 40$ GeV/c. Note that the parton level calculations of both double parton and double bremsstrahlung scattering cross sections are subject to large uncertainty due to our incomplete knowledge of structure functions at low Feynman x.

IX Conclusions

We have studied events containing four jets with corrected $p_T > 25$ GeV/c in $p\bar{p}$ collisions at $\sqrt{s} = 1.8$ TeV. We find that the p_T spectra and angular separation between any two jets in the event are in good agreement with the leading order QCD prediction for the double bremsstrahlung process. However, when variables more sensitive to the pairwise p_T balancing and angular distribution of the dijet pairs are used, a small double parton content provides the best fit to the data. The existence of clusters due to additional gluon radiation (five-jet events) was observed to be an important effect in determining this content. We

have used the double parton signal to measure both the double parton cross section $\sigma_{\rm DP}$ (for partons with $p_T > 18$ GeV/c) and the effective cross section $\sigma_{\rm eff}$. We find

$$\sigma_{\rm DP} = 63^{+32}_{-28}\ {\rm nb} \quad ({\rm parton}\ p_T > 18\ {\rm GeV/c}), \tag{27}$$

$$\sigma_{\rm eff} = 12.1^{+10.7}_{-5.4}\ {\rm mb}. \tag{28}$$

We also have placed the following bounds on $\sigma_{\rm eff}$:

$$4.1 < \sigma_{\rm eff} < 41\ {\rm mb} \quad (95\%\ {\rm C.L.}), \tag{29}$$

$$5.4 < \sigma_{\rm eff} < 29\ {\rm mb} \quad (90\%\ {\rm C.L.}). \tag{30}$$

Using the measured value $\sigma_{\rm eff} = 12.1$ mb, a Monte Carlo study has indicated that double parton scattering will be the dominant production mechanism for events containing four jets at the SSC ($\sqrt{s} = 40$ TeV), where the softest jet satisfies the requirement $p_T < 40$ GeV/c. This underscores the importance of the double parton scattering process as a background to any process leading to the production of four-jet events. The methods developed in this analysis will be immediately applicable to four-jet physics at the SSC and LHC. A quantitative measurement of parton correlations within the hadron should then become possible.

Acknowledgements

We thank the Fermilab staff and the technical staffs of the participating institutions for their vital contributions. We thank Dr. R. Carlitz for advice, encouragement and kind hospitality. This work was supported by the U.S. Department of Energy and National Science Foundation; the Italian Istituto Nazionale di Fisica Nucleare; the Ministry of Science, Culture, and Education of Japan; the National Science and Engineering Council of Canada; and the A. P. Sloan Foundation.

List of Tables

Table 1: Number of events remaining after each of the standard analysis cuts.

Cut	Events remaining
-	32738
$\mid z_{\rm vert} \mid < 60$ cm	30752
Four jets with $p_T^{\rm cor} > 25$ GeV/c	4408
Jet position $\mid \eta_d \mid < 3.5$	4404
Jet separation $\mid \Delta R \mid > 1.0$	3916
No secondary z-vertex	3113
$\sum p_T > 140$ GeV/c	2213

Table 2: Values obtained for the terms listed in Eq. 19, with associated uncertainties. We also include our determination of the dijet cross section, and the uncertainty on the dijet cross section caused by the jet energy scale uncertainty.

Term	Value	Uncertainty
$\mathcal{R}$	0.054	37%
$\mathcal{A}_{\rm DP}^{\rm cuts}$	6.5×10^{-3}	14%
$\mathcal{A}_{\rm DP}^{\rm trig}$	0.85	12%
$\mathcal{L}$	325 nb^{-1}	7%
Energy Scale	-	25%
$\sigma_{\rm dijet}$ (affects $\sigma_{\rm eff}$ only)	39 μb	20%

Table 3: A summary of the results, experimental parameters and event cuts for the double parton analyses performed by the AFS, UA2 and CDF collaborations.

	$\sqrt{s}$ (GeV)	$p_T^{\rm min}$ (GeV/c)	η Range	$N_{\rm events}$	Result
AFS	63	4	$\mid \eta \mid < 1$	$\sim 1,000$	$\sigma_{\rm eff} \sim 5$ mb
UA2	630	15	$\mid \eta \mid < 2$	$\sim 10,000$	$\sigma_{\rm eff} > 8.3$ mb (95% C.L.)
CDF	1800	25	$\mid \eta \mid < 3.5$	$\sim 2,000$	$\sigma_{\rm eff} = 12.1^{+10.7}_{-5.4}$ mb

List of Figures

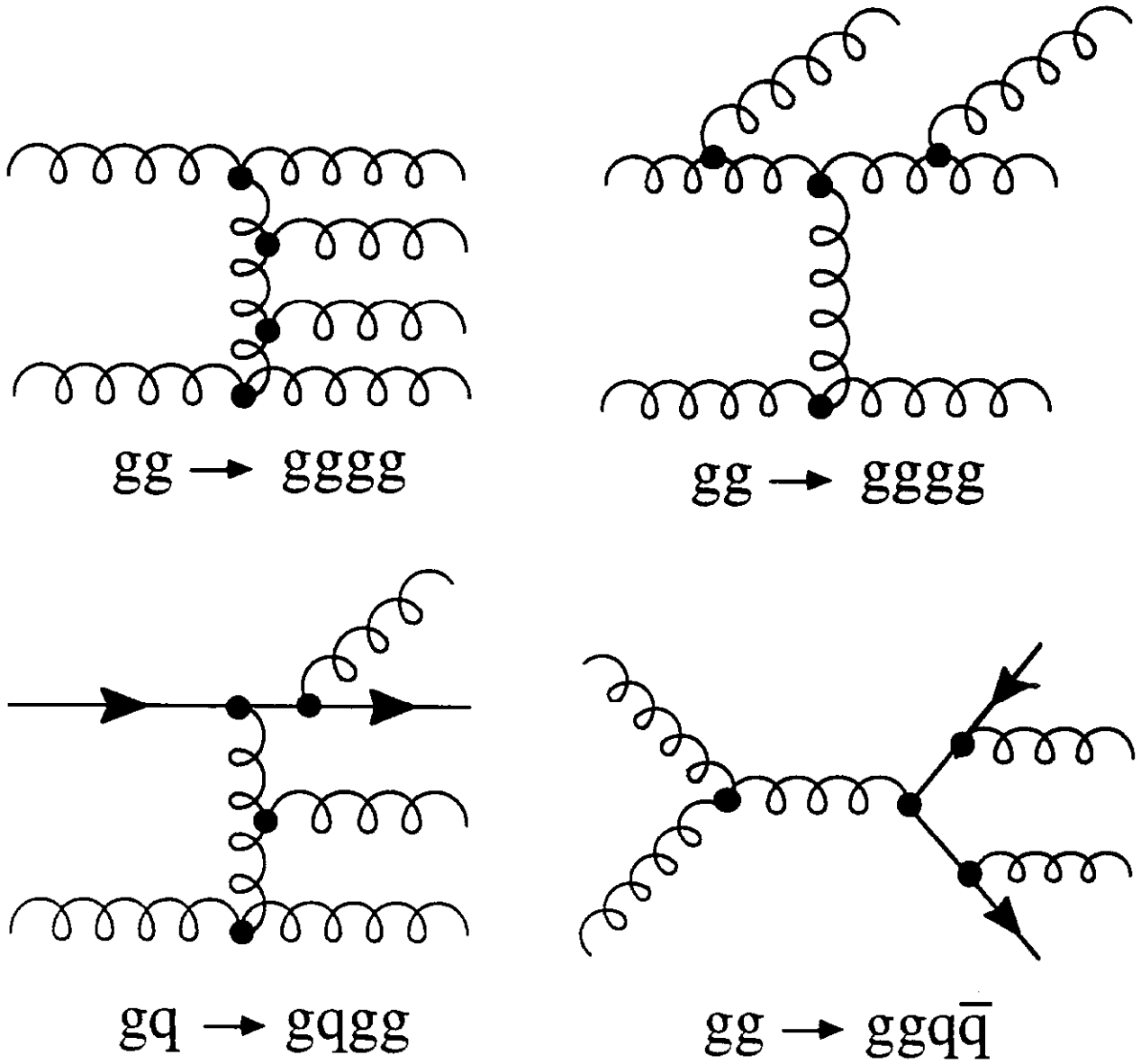

Figure 1: Four of the Feynman diagrams which contribute to the leading order matrix element expression for the double gluon bremsstrahlung process.

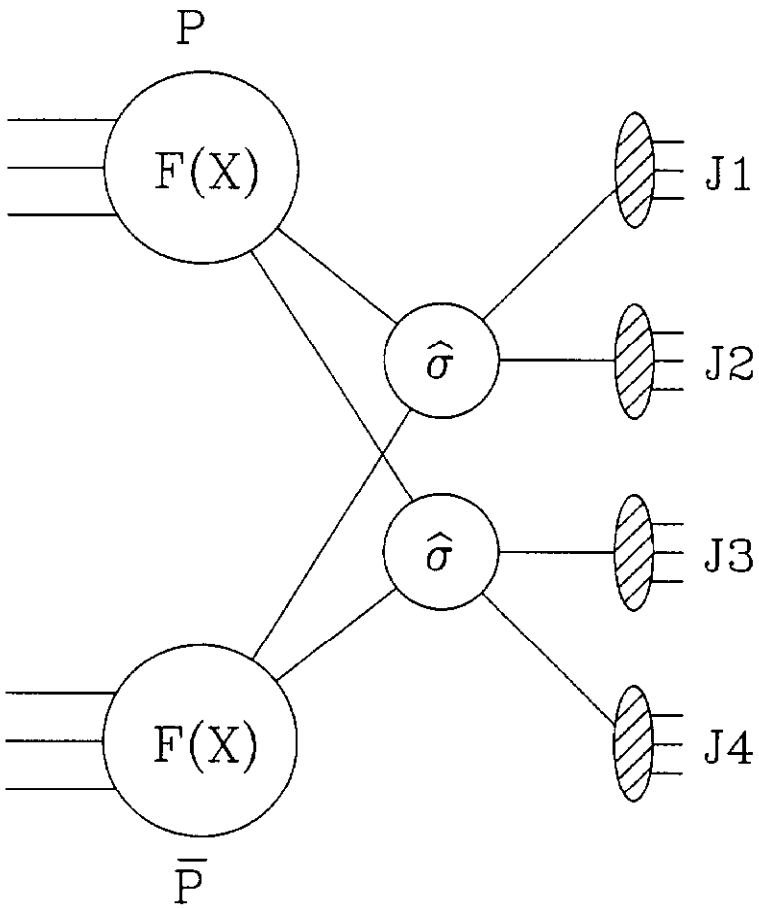

Figure 2: Schematic picture of the double parton scattering process, postulated to occur within a single hadron-hadron collision.

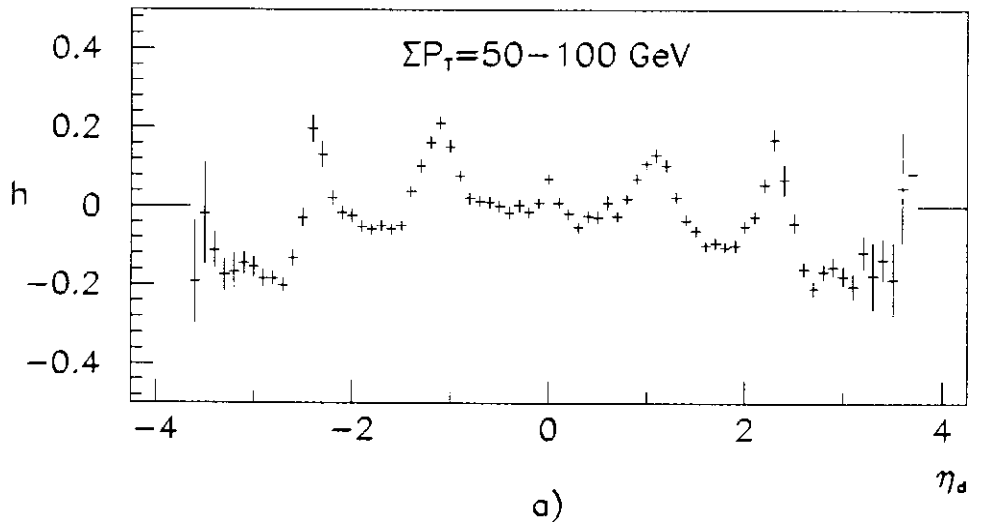

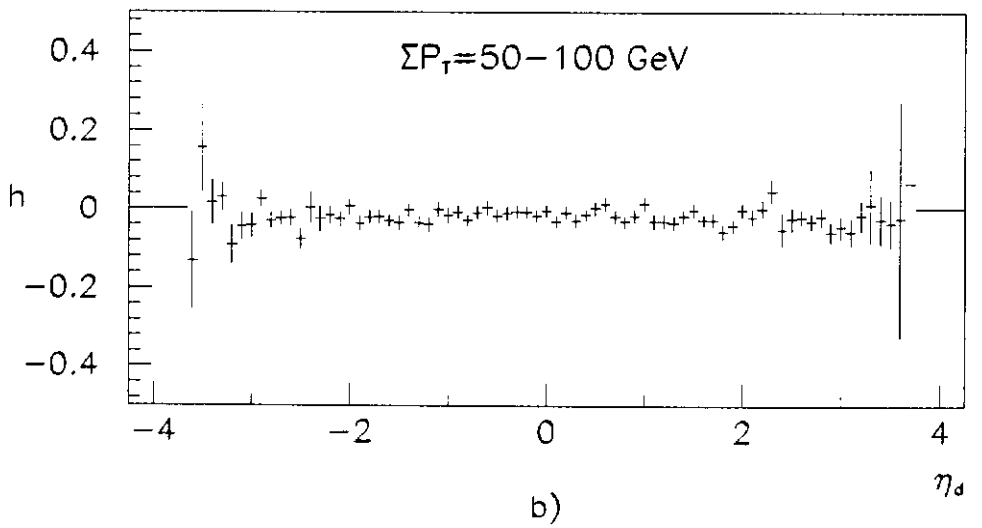

Figure 3: The projection fraction h (see text for definition) as a function of η_d for dijet data in the range $50 < \sum p_T < 100$ GeV/c a) before and b) after application of the relative jet correction.

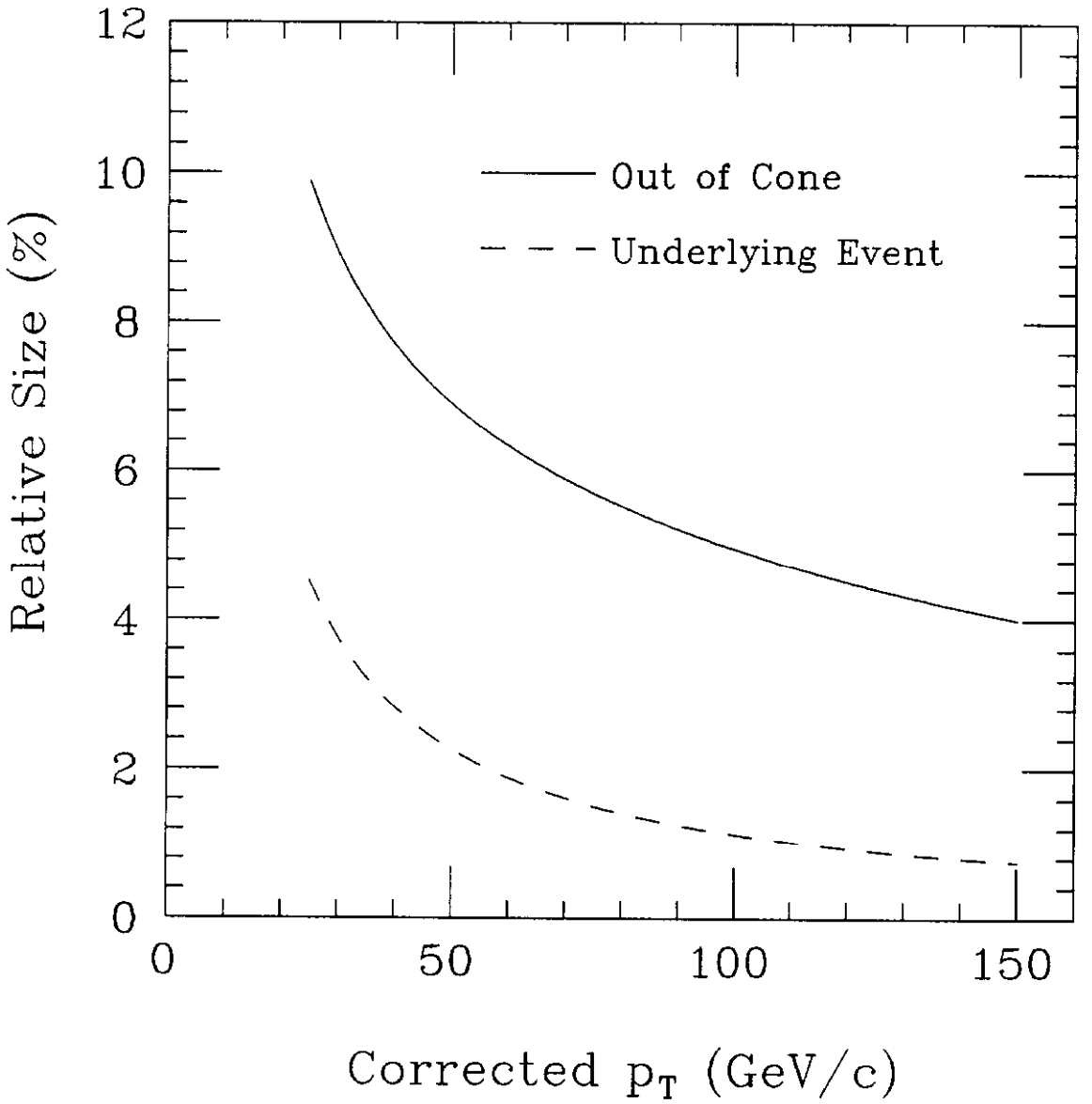

Figure 4: The ratio of out-of-cone and underlying event p_T to corrected jet p_T ($p_T^{\rm cor}$), as a function of corrected jet p_T. A cone of size 0.7 was used to define the jet.

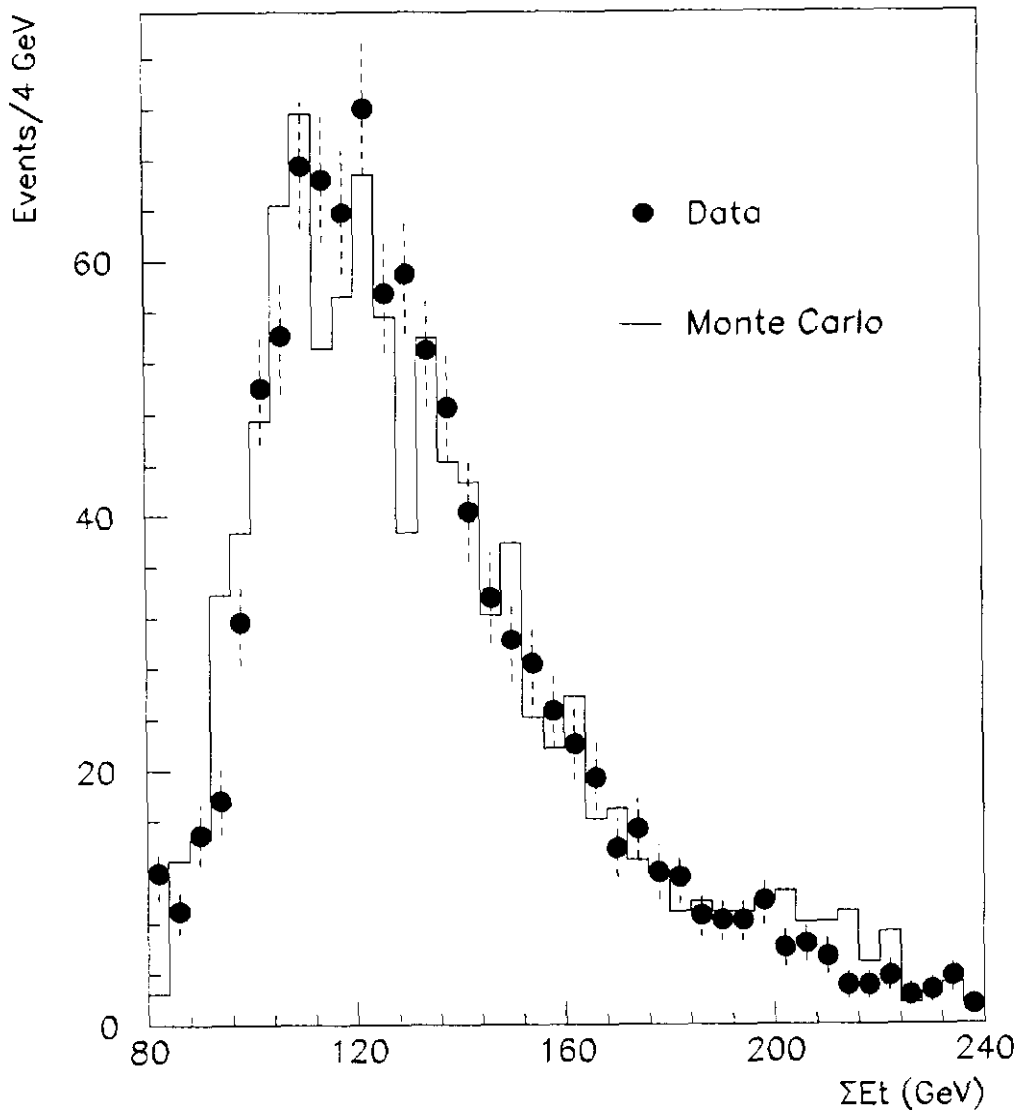

Figure 5: The level 2 trigger ΣE_T obtained with simulated four-jet events and full detector simulation, overlaid on the distribution obtained from four-jet data collected with the multijet trigger.

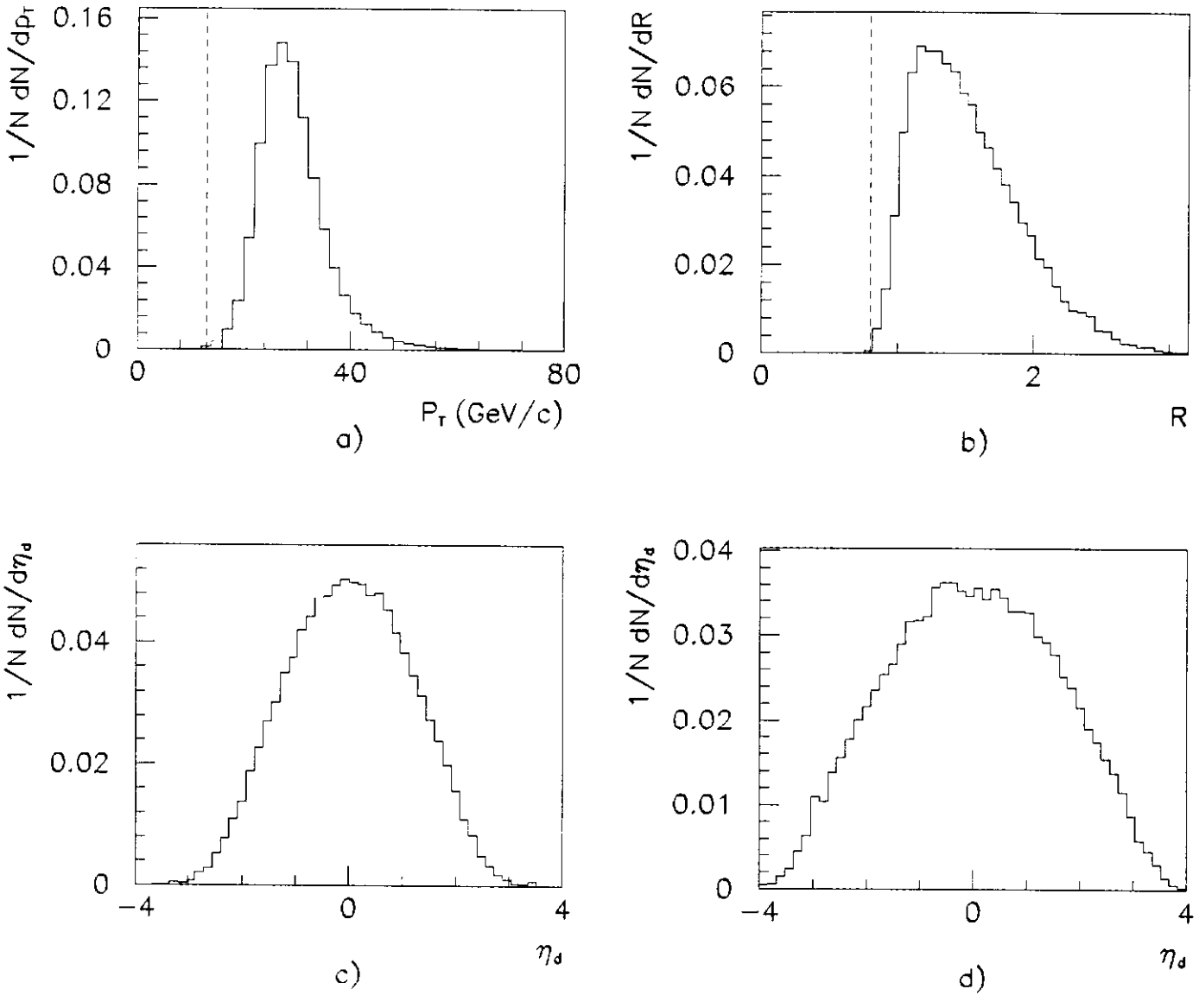

Figure 6: Distributions of a) softest parton p_T, b) minimum parton separation, c) and d) η_d of the highest and lowest p_T partons respectively for the double bremsstrahlung simulation. The fast jet simulation was used, and the standard offline cuts were applied to the corrected jets. The dashed lines shown in a) and b) indicate cuts at the events generator level.

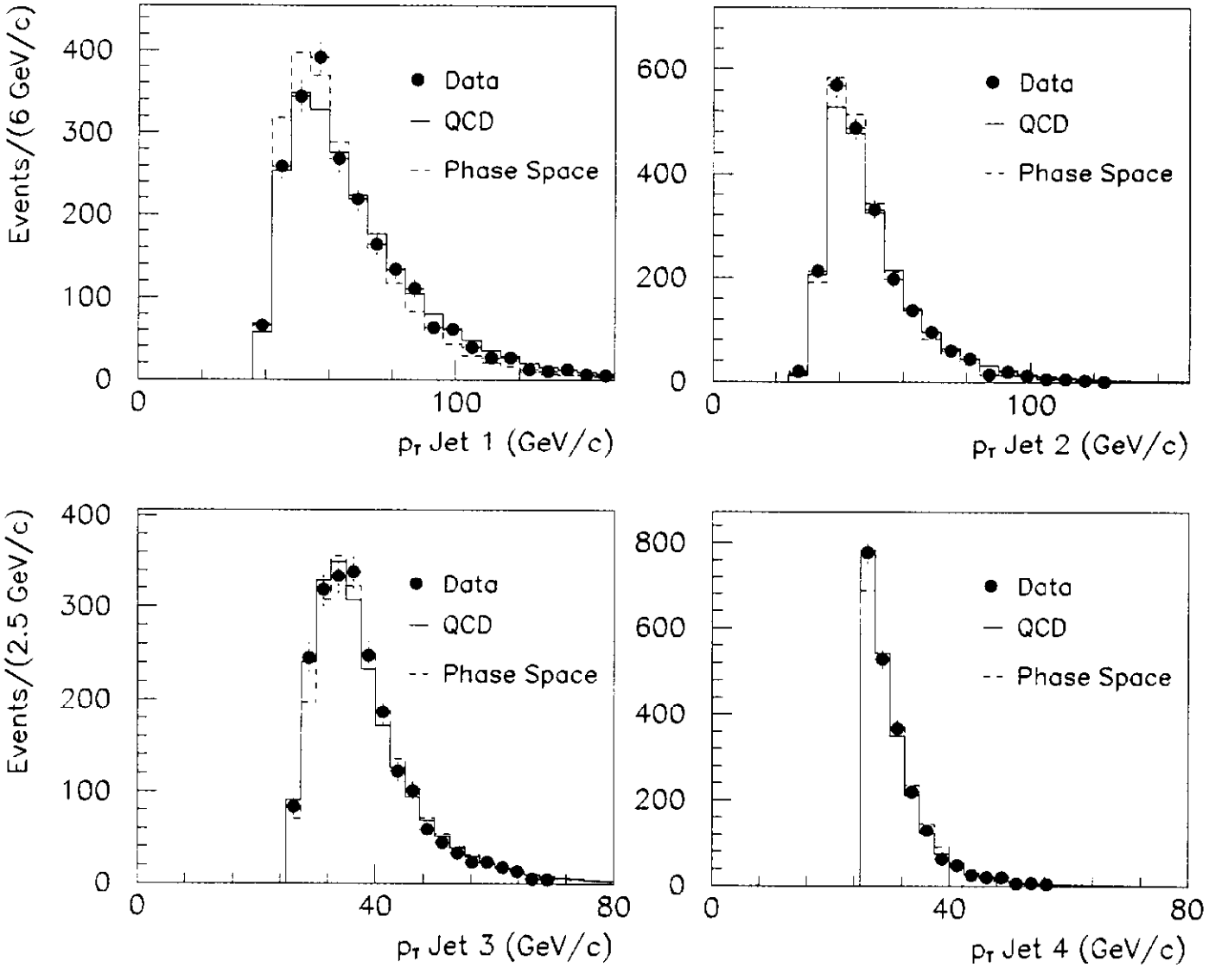

Figure 7: The p_T spectrum for all four jets obtained with data overlaid on the predictions of leading order QCD and four-body phase space. Jets are ordered by p_T, with jet 1 having the highest p_T, jet 2 having the next highest and so on.

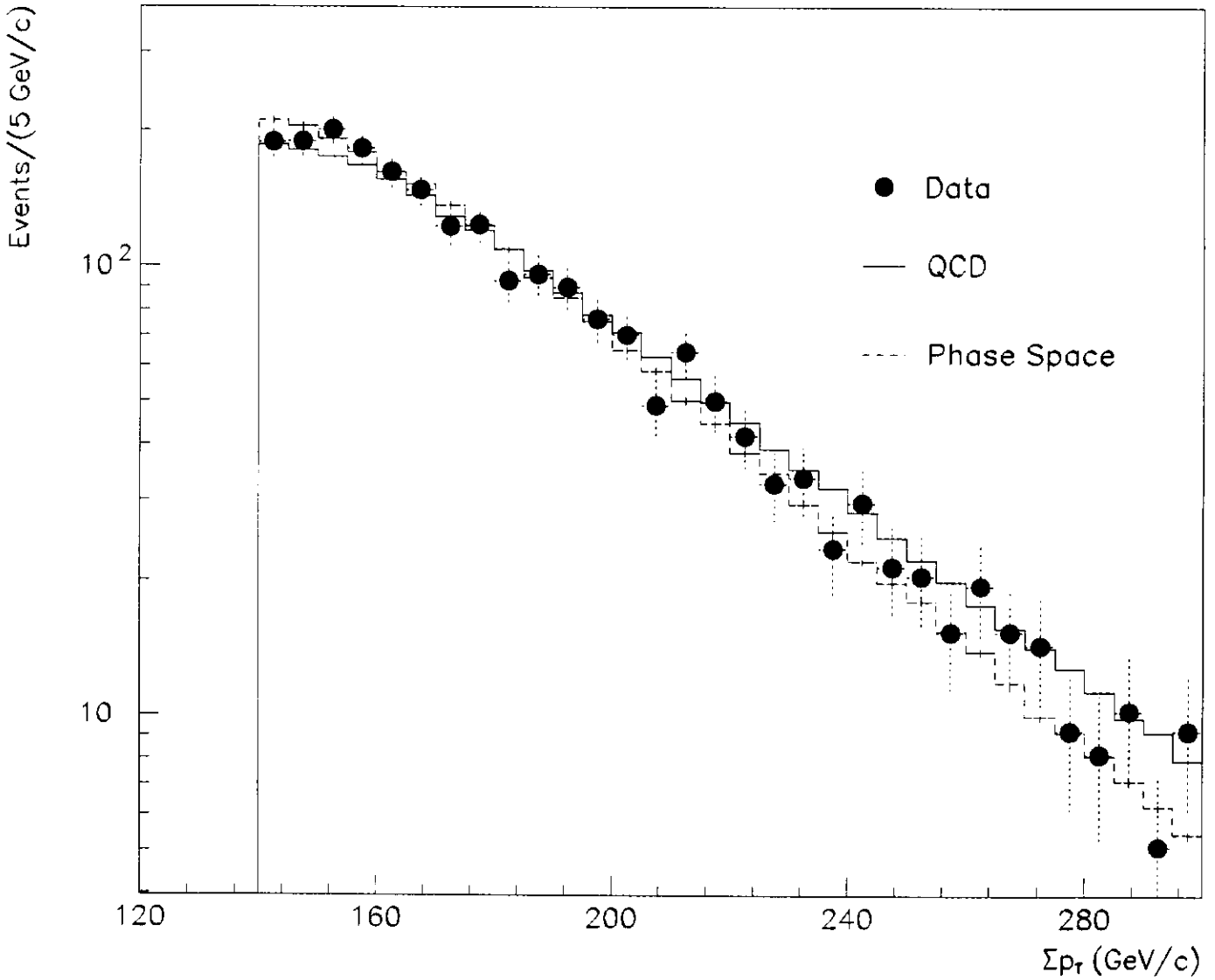

Figure 8: The scalar Σp_T spectrum for four-jet events obtained with data overlaid on leading order QCD and phase space distributions using structure function Morfin-Tung set 1 (DIS) with $Q = \langle p_T \rangle$.

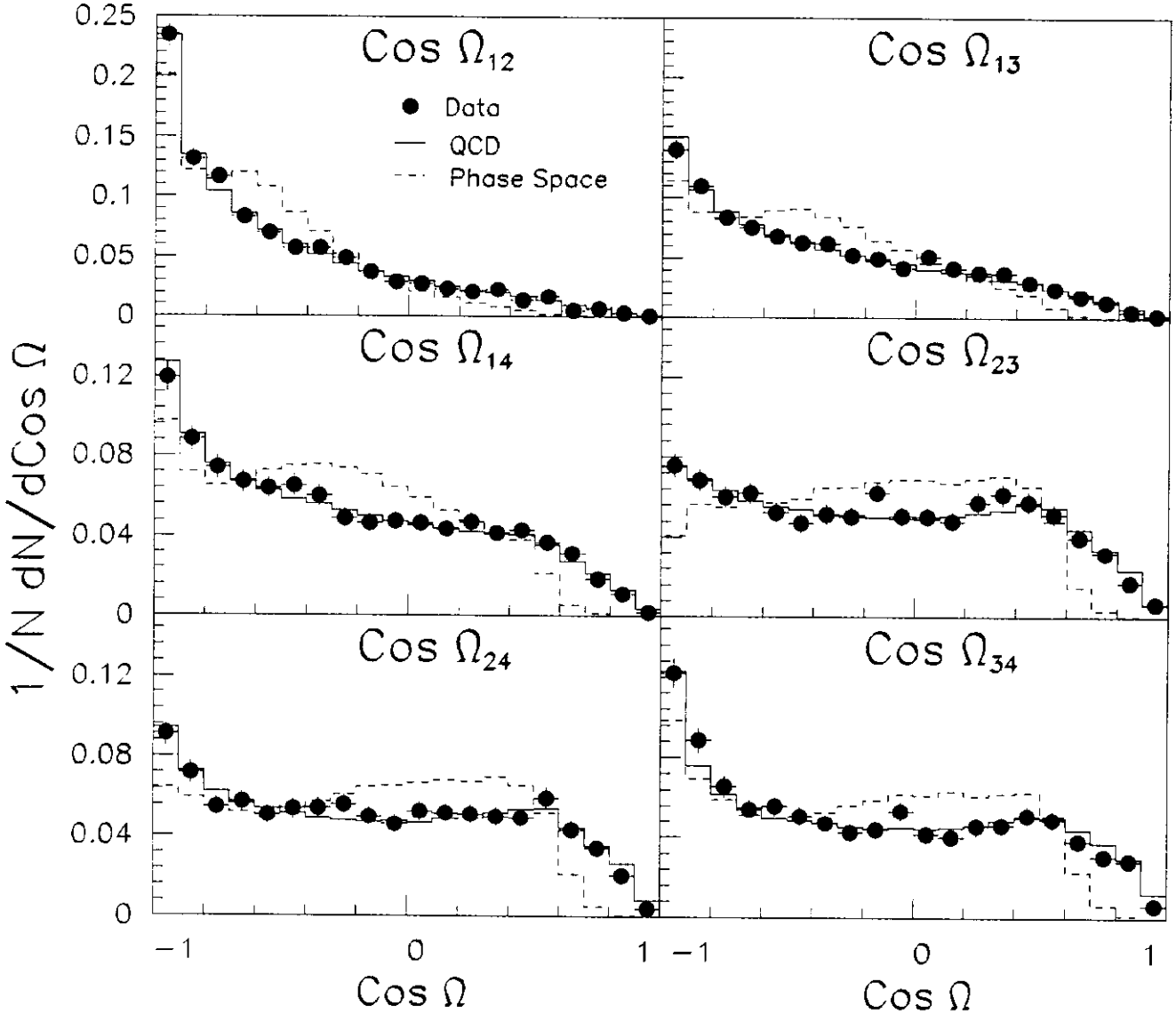

Figure 9: A comparison of data, QCD and phase space for the six angular variables $\cos\Omega_{ij}$ (defined in the text).

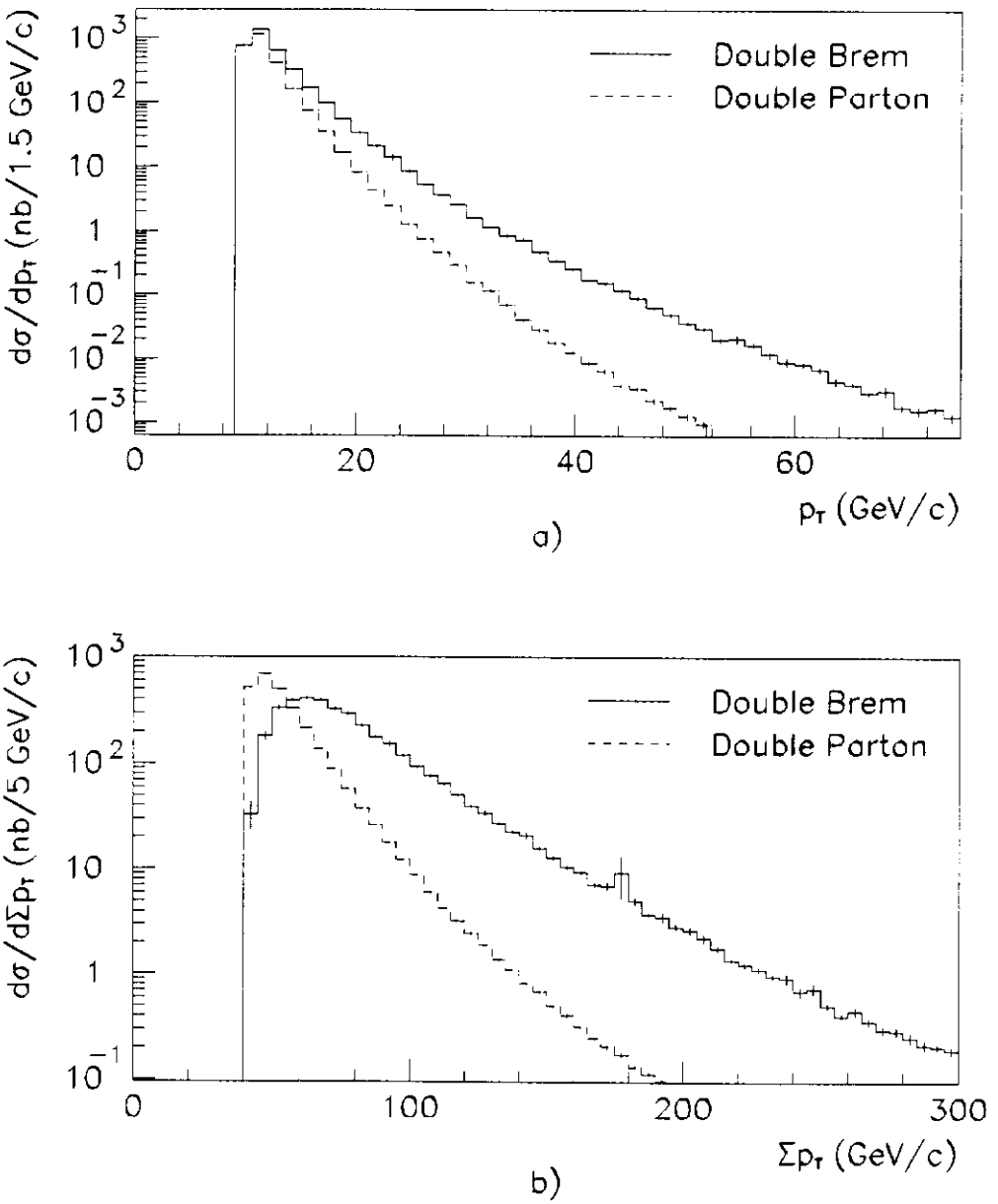

Figure 10: The double parton and double bremsstrahlung scattering cross sections plotted a) as a function of the p_T of the softest parton generated, b) as a function of the scalar Σp_T of all four jets. A value of $\sigma_{\rm eff} = 10$ mb has been used in the double parton calculation, with structure function set EHLQ1, $Q = \langle p_T \rangle$.

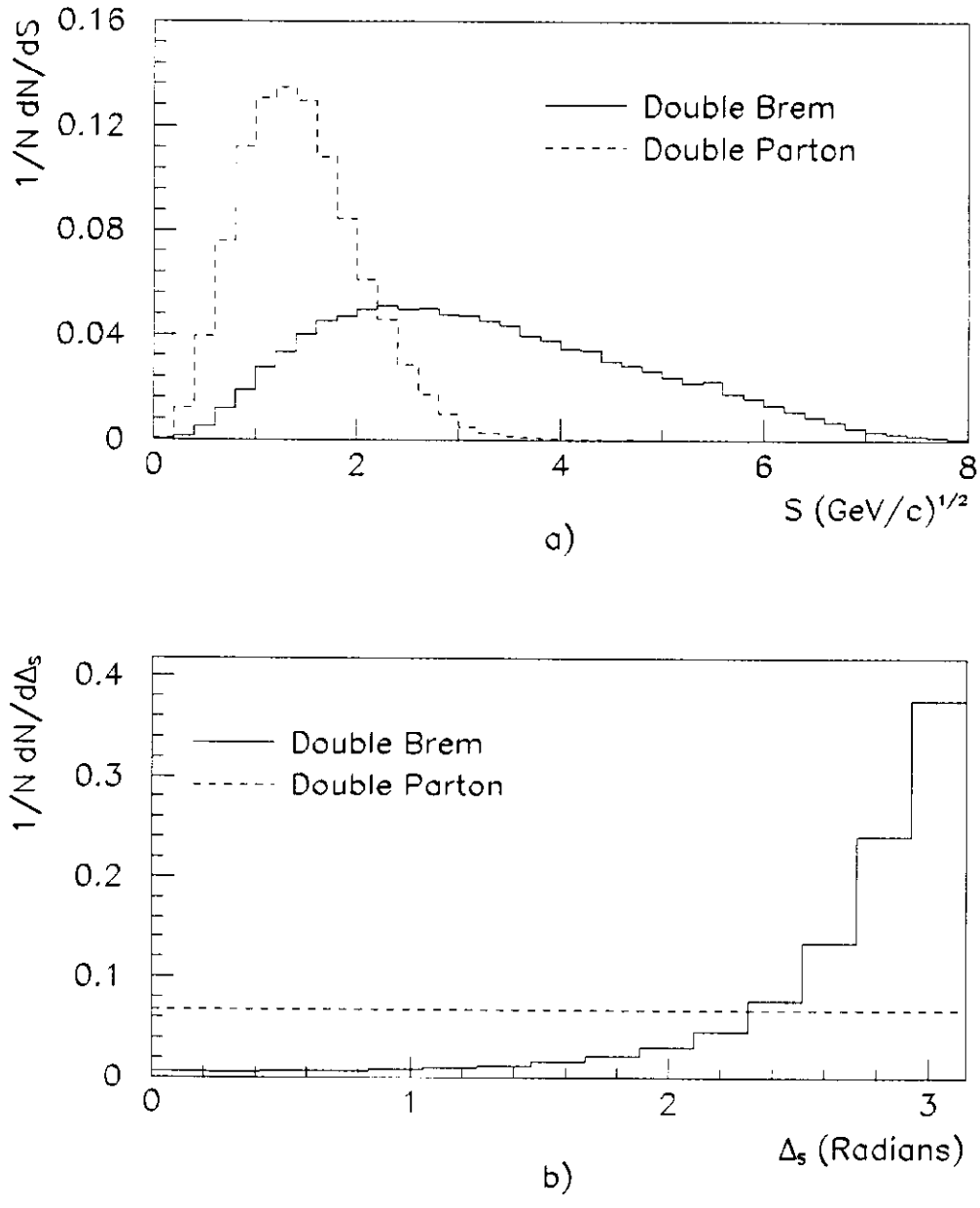

Figure 11: The distributions of a) S and b) Δ_S for double parton and double bremsstrahlung simulated events. Detector effects have been modeled using the fast jet simulation.

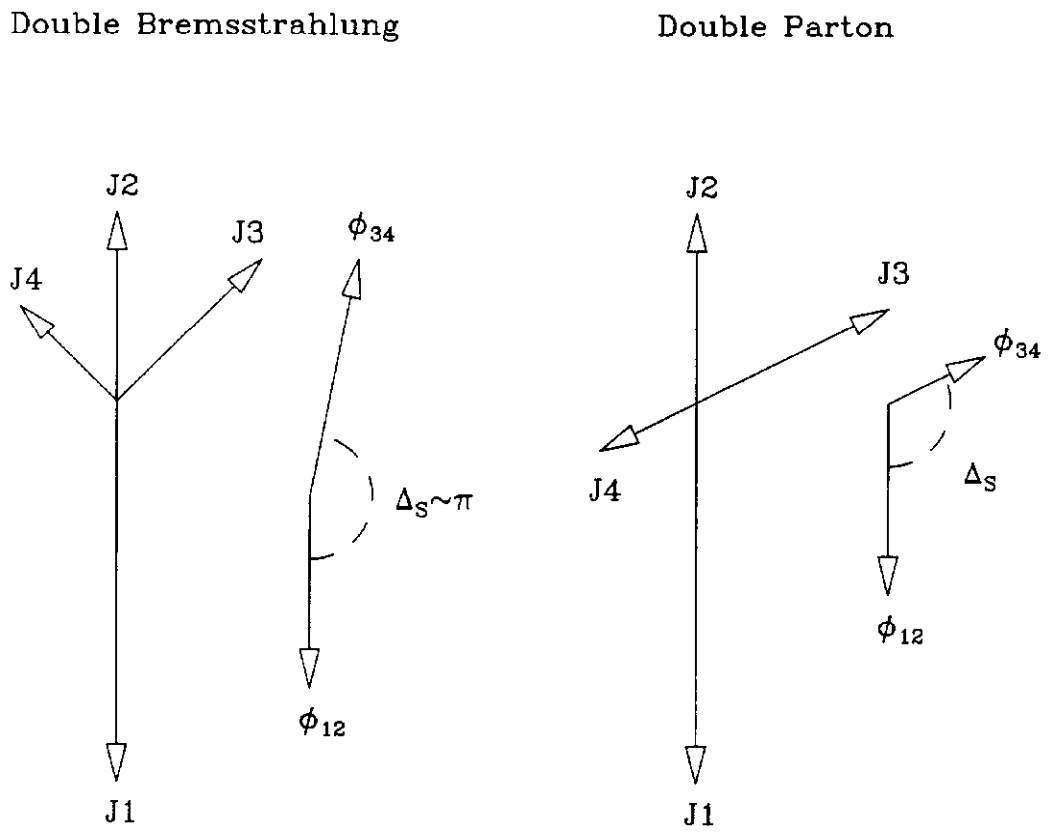

Figure 12: The Δ_S variable (defined in the text) for typical double bremsstrahlung (left) and double parton (right) jet configurations. In the case of double bremsstrahlung events, $\Delta_S \sim \pi$. The pairing of jets according to p_T-balancing gives a uniform distribution for double parton events.

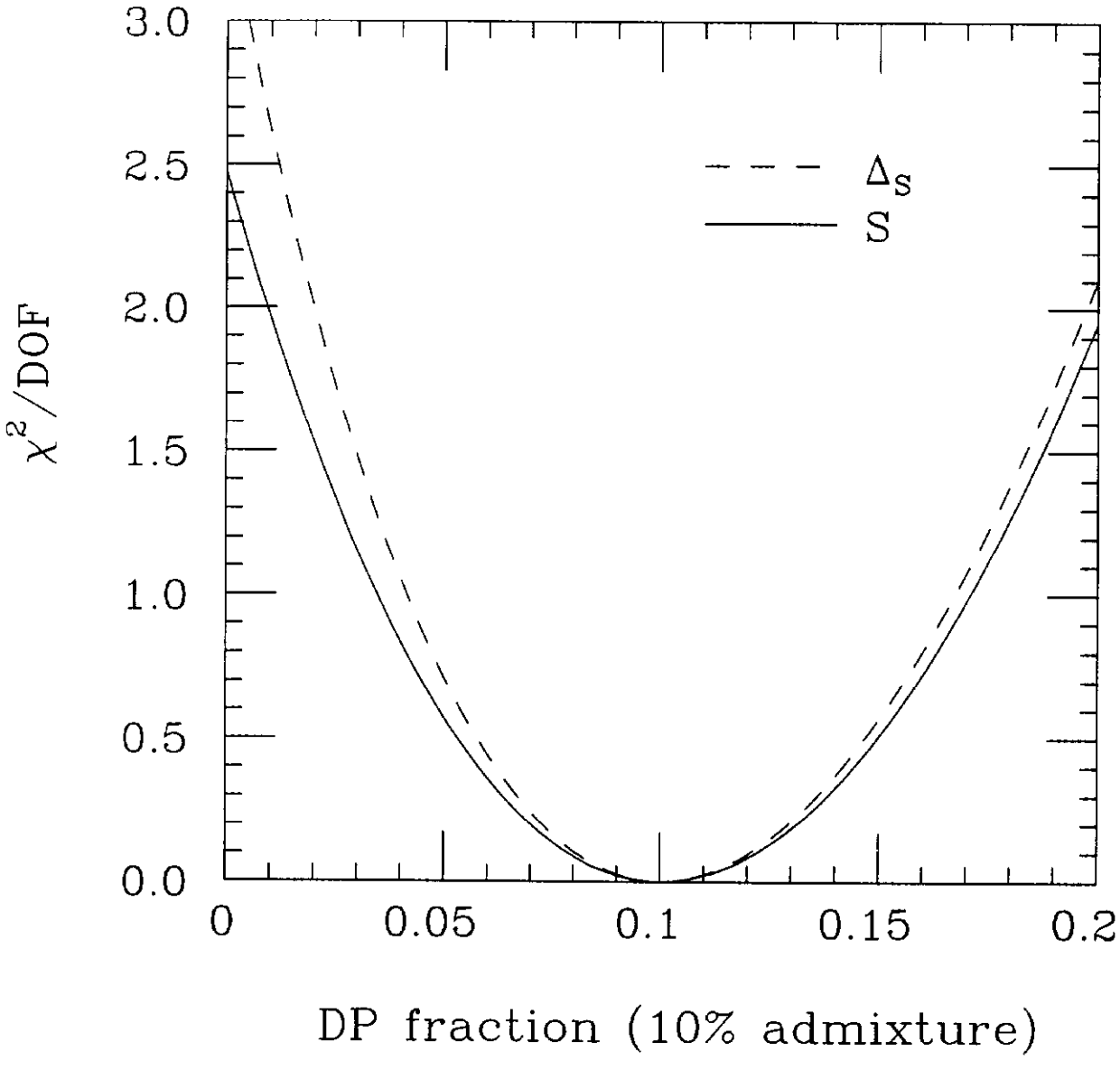

Figure 13: The χ^2_r dependence of S and Δ_S as a function of the fraction of double parton events for a Monte Carlo sample of 90% double bremsstrahlung and 10% double parton events.

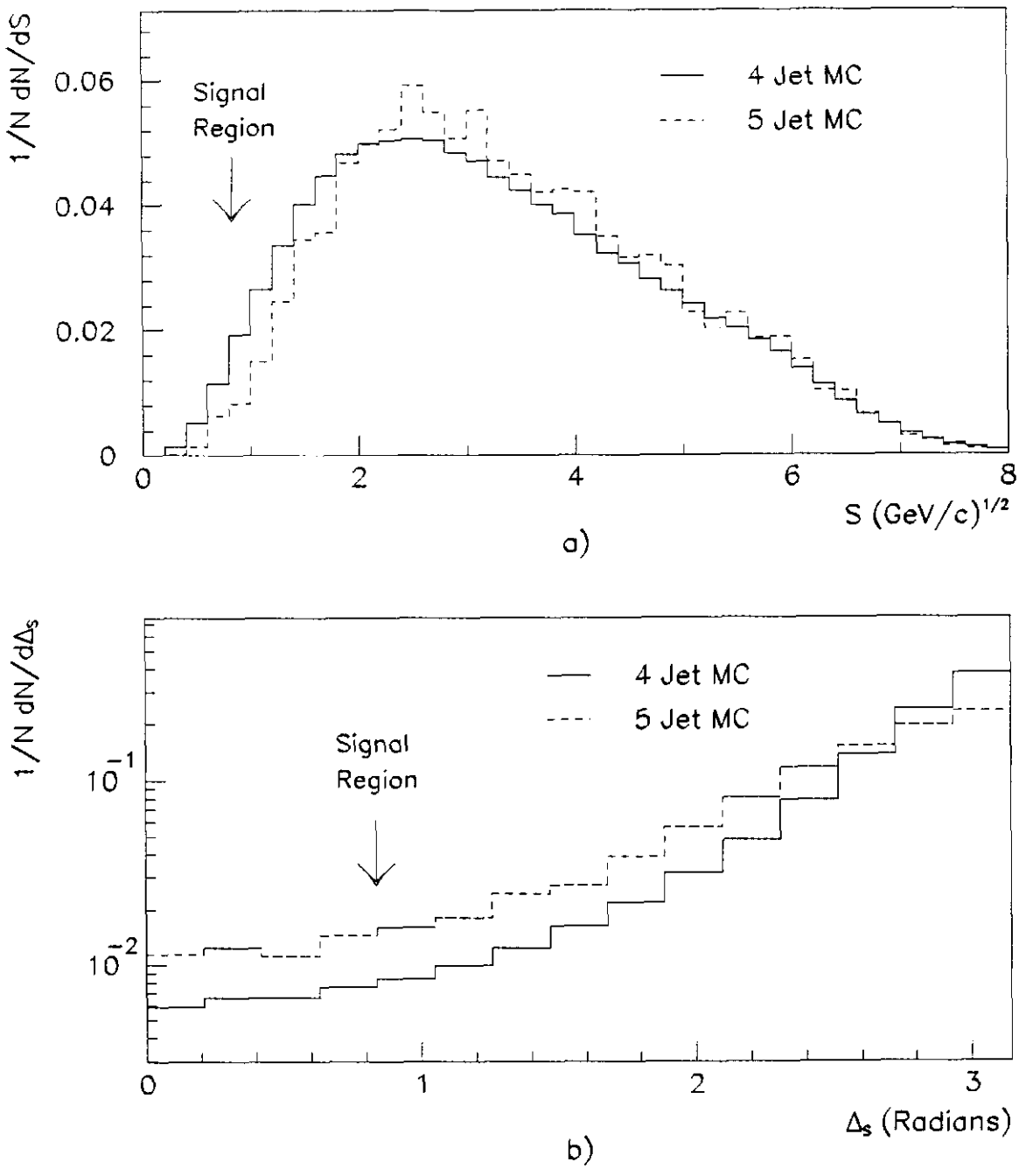

Figure 14: Distributions of a) S and b) Δ_S obtained using simulated five-jet events, where only four jets pass the standard analysis cuts. For comparison, the distributions obtained with the four-jet simulation are also shown. The Δ_S distribution is shown using a logarithmic scale for clarity.

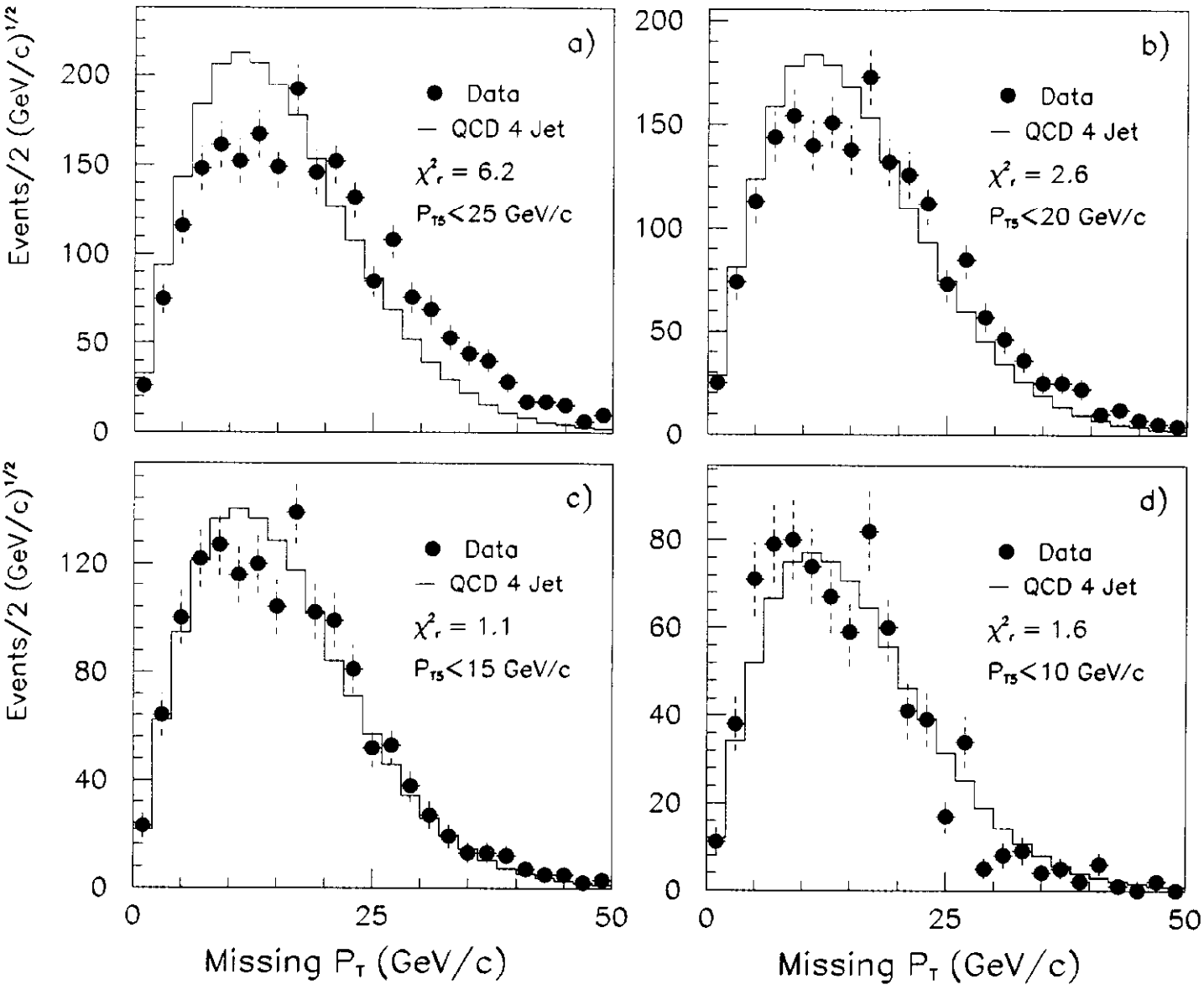

Figure 15: Missing p_T calculated using the vector sum of the leading four jets. Data points are shown for the cuts a) $p_{T5} < 25$ GeV/c, b) $p_{T5} < 20$ GeV/c, c) $p_{T5} < 15$ GeV/c and d) $p_{T5} < 10$ GeV/c compared to the Monte Carlo double bremsstrahlung prediction. Note that the double bremsstrahlung simulation produces four jets exclusively.

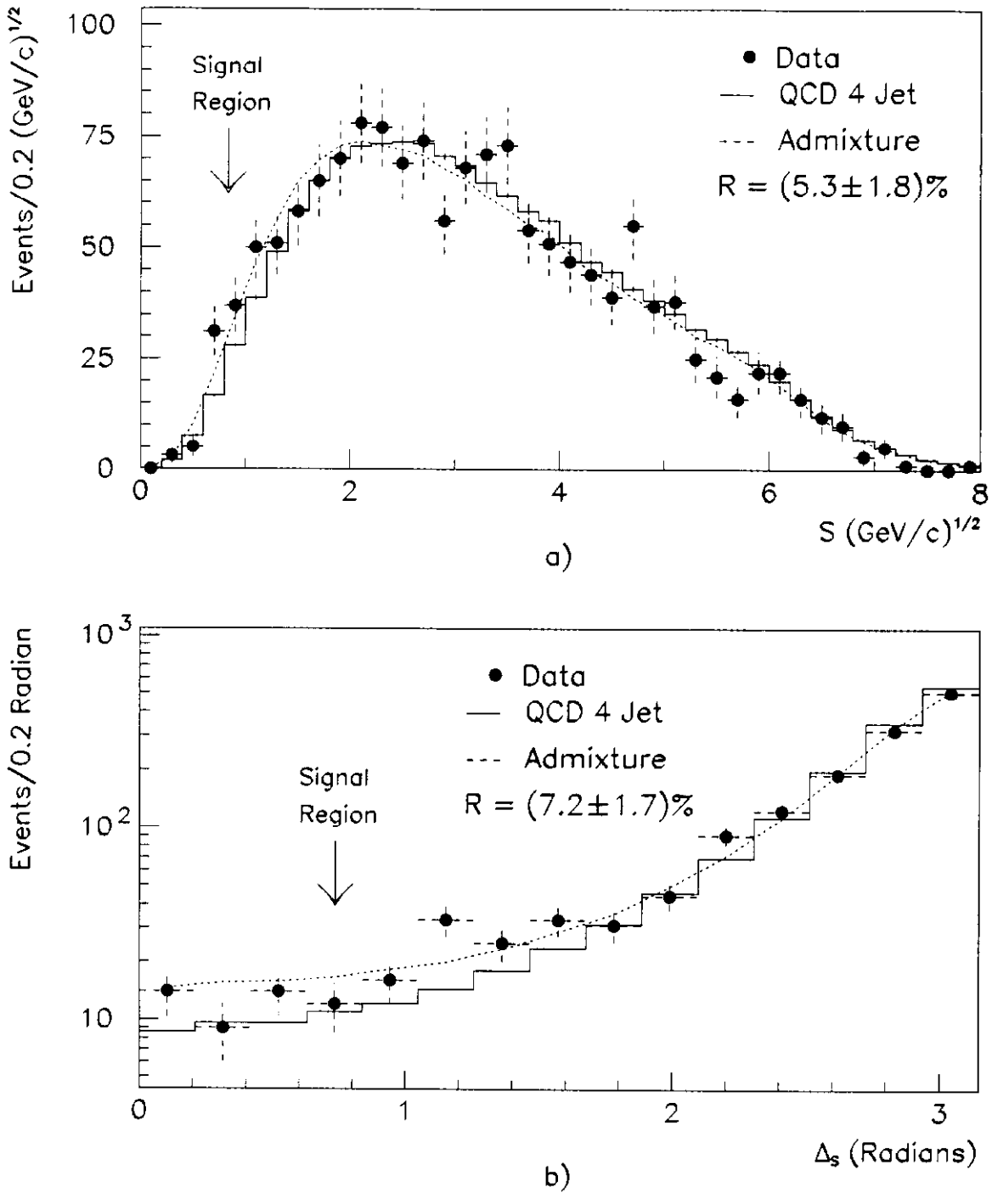

Figure 16: Distributions of a) S and b) Δ_S obtained using four-jet data with a cut on fifth jets of $p_{T5} < 15$ GeV/c overlaid on the QCD double bremsstrahlung distribution and a fitted admixture of double bremsstrahlung and double parton distributions. Also shown are the fitted values of $\mathcal{R}$. The Δ_S distribution is shown using a logarithmic scale for clarity.

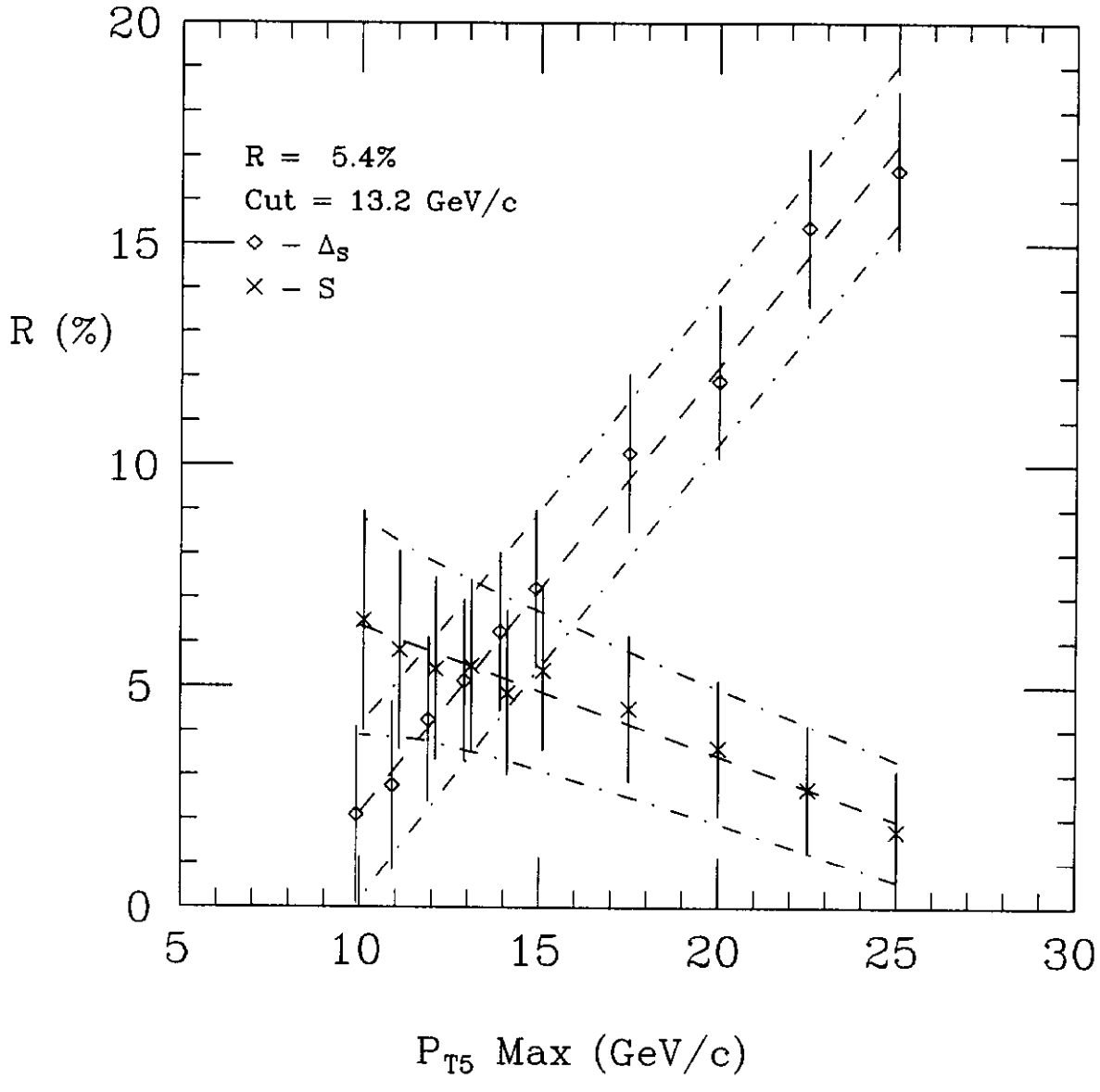

Figure 17: The calculated double parton fraction in CDF four-jet data $\mathcal{R}$ (see text for definition) for the S and Δ_S variables as a function of cut on the p_T of the fifth jet.

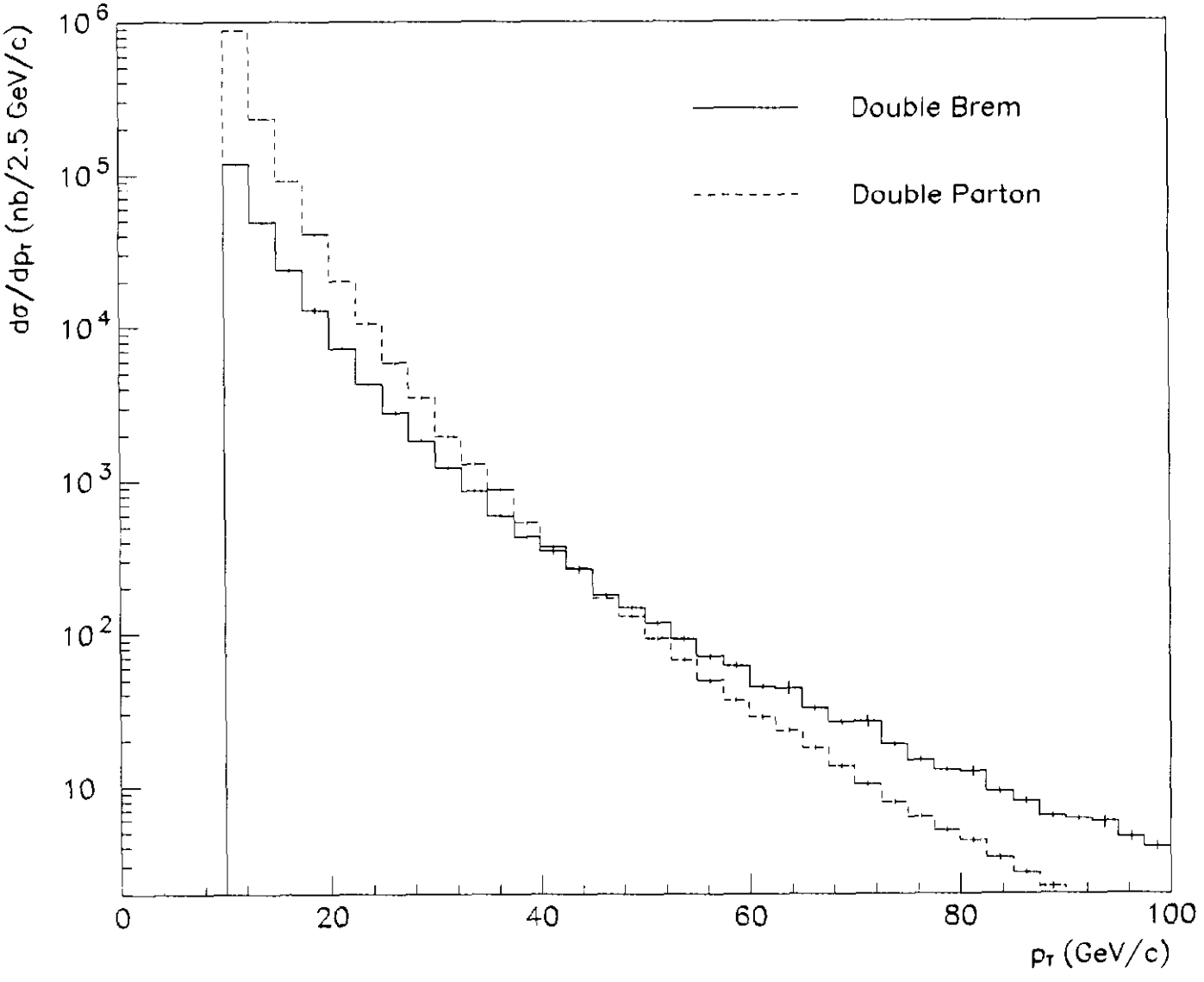

Figure 18: The double parton and double bremsstrahlung cross sections at $E_{CM} = 40$ TeV as a function of the p_T of the softest parton. We have used $\sigma_{\text{eff}} = 12.1$ mb. Our choice of structure function is Morfin-Tung set 1 (DIS), with $Q = \langle p_T \rangle$.

References

[a] Visitor.

[1] J. Gunion and Z. Kunszt, Phys. Lett. B **159**, 167 (1985); S. Parke and T. Taylor, Nucl. Phys. B **269**, 410 (1986); Z. Kunszt, Nucl. Phys. B **271**, 333 (1986); J. Gunion and Z. Kunszt, Phys. Lett. B **176**, 163 and 477 (1986); J. Gunion and J. Kalinowski, Phys. Rev. D **34**, 2119 (1986); S. Parke and T. Taylor, Phys. Rev. D **35**, 313 (1987); F.A. Berends and W. Giele, Nucl. Phys. B **294**, 700 (1987); M. Mangano, S. Parke and Z. Xu., Nucl. Phys. B **298**, 673 (1988); M. Mangano and S. Parke, Nucl. Phys. B **299**, 190 (1987).

[2] Z. Kunszt, Phys. Lett. B **145**, 132 (1984); Z. Kunszt and W.J. Stirling, Phys. Lett. B **171**, 307 (1986); L. Ametller, N. Paver and D. Treleani, Phys. Lett. B **169**, 289 (1986).

[3] R.D.Carlitz, *Parton Correlation Functions*, University of Pittsburgh preprint PITT-88-05 (1989), unpublished.

[4] AFS collaboration, T. Åkesson *et al.*, Z. Phys. C **34**, 163 (1987).

[5] UA2 collaboration, J. Alitti *et al.*, Phys. Lett. B **268**, 145 (1991).

[6] CDF collaboration, F. Abe *et al.*, Phys. Rev. D. **44**, 29 (1991).

[7] T. Sjostrand and M. van Zijl, Phys. Rev. D**36**, 2019 (1987).

[8] Yu L. Dokshitzer, Zh. Eksp. Teor. Fiz. **73**, 1216 (1977).

[9] CDF collaboration, F. Abe *et al.*, Nucl. Instrum. Methods A **267**, 272 (1988).

[10] F. Snider *et al.*, Nucl. Instrum. Methods A **268**, 75 (1988).

[11] D. Amidei *et al.*, Nucl. Instrum. Methods A **269**, 51 (1988).

[12] J.T. Carrol *et al.*, Nucl. Instrum. Methods A **300**, 552 (1991).

[13] CDF collaboration, F. Abe *et al.*, Phys. Rev. D **45**, 1448 (1992).

[14] G. Sterman and S. Weinberg, Phys. Rev. Lett. **39**, 1436 (1977).

[15] F. Aversa *et al.*, Phys. Lett. B **210**, 225 (1988).

[16] S. Ellis, Z. Kunszt, and D. Soper, Phys. Rev. Lett. **62**, 2188 (1989).

[17] L. Keeble, *A Study of Four-Jet Events and Search for Double Parton Interactions with the Collider Detector at Fermilab*, Ph.D. dissertation, Texas A&M University (1992, unpublished).

[18] CDF collaboration, F. Abe *et al.*, Phys. Rev. D **45**, 3921 (1992).

[19] R. Field and R. Feynman, Nucl. Phys. B **136**, 1 (1978).

[20] F. Paige and S. Protopopescu, Report No. BNL-38034, 1986 (unpublished); *Physics of the Superconducting Super Collider, Snowmass,* 1986, Proceedings of the Summer Study, Snowmass, Colorado, 1986, edited by R. Donaldson and J. Marx (Division of Particles and Fields of the APS, New York, 1987), p. 320. We used the fragmentation model contained within the ISAJET Monte Carlo program tuned to agree with dijet data.

[21] CDF collaboration, *A Comparison of Jet Production in $p\bar{p}$ Collisions at $\sqrt{s} = 546$ and 1800* GeV, submitted to Phys. Rev. Lett.

[22] CDF collaboration, F. Abe *et al.*, Phys. Rev. Lett. **68**, 1104 (1992).

[23] Z. Kunszt and W.J. Stirling, Phys. Rev. D **37**, 36 (1988).

[24] Ian Hinchliffe, private communication. Version 3.65 was used.

[25] J. Morfin and W.K. Tung, Zeit. Phys. C **52**, 13 (1991).

[26] J. Patrick, *Dijet Angular Distribution and Multijet topology at $\sqrt{s} = 1.8$* TeV, Proceedings of the 7th Topical Workshop on Proton-Antiproton Collider Physics, Fermilab, Batavia, Illinois, U.S.A., 20–24 June 1988, eds. R. Raja, A. Tollestrup and J. Yoh, p. 217.

[27] C.J. Maxwell, Phys. Lett. B **192**, 190 (1987).

[28] M. Diemoz, F. Ferroni, E. Longo and G. Martinelli, Z. Phys. C**39**, 21 (1988).